Eur. Phys. J. B **10**, 739–760 (1999)

THE EUROPEAN PHYSICAL JOURNAL B

EDP Sciences
© Società Italiana di Fisica
Springer-Verlag 1999

Bose-Einstein condensation in interacting gases

M. Holzmann[1,2], P. Grüter[1,a], and F. Laloë[1,2,b]

[1] LKB[c] and LPS[d], Département de Physique de l'ENS, 24 rue Lhomond, 75005 Paris, France
[2] Institute of Theoretical Physics, UCSB, Santa Barbara, CA 93106, USA

Received 13 November 1998

Abstract. We study the occurrence of a Bose-Einstein transition in a dilute gas with repulsive interactions, starting from temperatures above the transition temperature. The formalism, based on the use of Ursell operators, allows us to evaluate the one-particle density operator with more flexibility than in mean-field theories, since it does not necessarily coincide with that of an ideal gas with adjustable parameters (chemical potential, etc.). In a first step, a simple approximation is used (Ursell-Dyson approximation), which allow us to recover results which are similar to those of the usual mean-field theories. In a second step, a more precise treatment of the correlations and velocity dependence of the populations in the system is elaborated. This introduces new physical effects, such as a change of the velocity profile just above the transition: the proportion of atoms with low velocities is higher than in an ideal gas. A consequence of this distortion is an increase of the critical temperature (at constant density) of the Bose gas, in agreement with those of recent path integral Monte-Carlo calculations for hard spheres.

PACS. 05.30.Jp Boson systems – 05.30.-d Quantum statistical mechanics – 03.75.Fi Phase coherent atomic ensembles; quantum condensation phenomena

1 Introduction

The notion of Bose-Einstein condensation is not new: it was introduced by Einstein in 1925 [1]; Bose himself played an important role in the introduction of Bose-Einstein statistics, but his work was focussed on radiation (photons) – he did not generalize it to massive particles and therefore played no role in the discovery of the phase transition [2,3]. It is well-known that, for many years, the so called "Einstein phenomenon" [4] was considered more as a mathematical artifact of the formalism than a physical reality – this was for instance the case of Uhlenbeck himself [5–7]. Indeed, this reaction is perfectly natural: the notion of accumulating particles into one single quantum state – with no limit on the accuracy of the definition of their momentum, except the size of the macroscopic container – looks rather paradoxical at first sight. For an ideal gas, it certainly introduces unphysical properties: density profiles which depend critically on the boundary conditions of the wave functions on the walls, in violation of extensivity [8], or anomalous fluctuations of particle numbers, which become ensemble dependent [9–11]. It is now well understood that these pathological features disappear as soon as some repulsive interaction between the particles is added; but then, by naive analogy, one could ask why the occupancy of a single quantum state does not disappear as well? After all, it would also seem perfectly natural to assume that, in an interacting system, some finite momentum band is highly populated[1]. How can we show, from *ab initio* arguments, that the accumulation of a finite proportion of particles into a single quantum state is indeed a robust property against the presence of interactions?

Curiously, in view of the importance of the phenomenon, the literature contains relatively little discussion of this question and of the possibility of what has sometimes be called "fractionned" or "smeared" boson condensates; in particular, following London's historical intuition [12], most textbooks prefer to simply assume that one single state is populated macroscopically, and then proceed to study the interesting consequences of this Ansatz. At zero temperature, a general argument was

[a] *Present address*: McKinsey and Company, Kurfürstendamm 185, 10707 Berlin, Germany.
[b] e-mail: laloe@ens.fr
[c] The Laboratoire Kastler Brossel is Unité Associée au CNRS (UA 18) et à l'Université Pierre et Marie Curie.
[d] The Laboratoire de Physique Statistique de l'ENS is Unité Associée au CNRS (UA 1306) et aux Universités Paris 6 et Paris 7.

[1] An elementary idea, for instance, would be to suggest that the width of the band is related by some inverse Fourier relation to the mean-free-path in the gas.

nevertheless given by Penrose and Onsager[2] in 1956 [13]; other famous references are the work of Beliaev [14], Yang [15], Gavoret *et al.* [16] and of Fröhlich [17]; in 1962, Girardeau [18] discussed in detail the possibility of what he called a "generalized condensation, where no one single-particle state is macroscopically occupied"; a more recent discussion was given by Nozières [19], who concluded from a Hartree-Fock calculation at zero temperature that repulsive interactions tend to stabilize the single state occupancy. At finite temperatures, "smeared condensation" was discussed explicitly in an article by Luban in 1962 [20] and, more recently and in a mean field context, by Van den Berg *et al.* [21]. There is also a large amount of beautiful numerical work on the subject [22], which leads to an impressive agreement with experimental data, in particular in liquid helium four; but one should keep in mind that numerical methods are subject to limitations due to finite size effects in the evaluation of narrow peaks in occupation numbers. For a critical discussion of experimental evidence for a condensate in superfluid helium four, see for instance Sokol [23].

Two general remarks may come to mind at this stage. The first is that it is known, from very general considerations, that the Bose-Einstein statistics plays no role whatsoever at zero temperature (Boltzmann and Bose Einstein systems have exactly the same ground state); zero temperature arguments therefore do not directly address the question of how the statistics is able to stabilize the single state occupancy against finite temperature excitations. The second is that mean-field (Hartree-Fock) arguments are based on an approximation where the system is considered as equivalent to a gas of independent particles with modified parameters, which automatically preserves the main properties of the ideal gas (for which the occurrence of Bose-Einstein condensation depends only on the density of states at the origin); they do not really address the question of the robustness of single state occupancy against all kinds of correlation that can be created in a system by interactions, but rather assume it. A theoretical study where the property in question would not be an ingredient, but a consequence of the results of the calculations, could therefore be useful.

There are also other issues which are not completely settled, such as the effects of the interactions on the transition temperature itself. For instance one may ask if repulsive hard cores with short range will tend to increase or to decrease the critical temperature (at constant density[3]). In 1957, the method of pseudopotentials [25,26] was applied by Huang and coll. to the study of the properties of the phase transition in Bose hard spheres. The result is that the critical temperature should be slightly increased (by an amount proportional to $a^{3/2}$, where a is the diameter of the spheres); see also reference [27]. The physical interpretation given by the authors is that, by a Heisenberg type relation, "a spatial repulsion gives rise to a momentum space attraction", therefore facilitating the appearance of a condensate. But, since then, other methods of approach to the problem have been proposed, in particular a Hartree-Fock type approximation [28]. It turns out that this method provides the opposite result: a purely repulsive potential is predicted to lower the transition temperature! More precisely, it predicts that the change in T_c depends essentially on the range of the potential (it vanishes for a contact potential) and that, for most of repulsive potentials with finite range (a "top hat potential" for instance) the exchange interaction tends to increase the effective mass of the particles and therefore to lower T_c. Of course, this does not necessarily mean that the two results are contradictory: each of them might be correct in a different domain[4]. Later,

[2] Penrose and Onsager were the first to define the phenomenon of Bose-Einstein condensation in an interacting system in terms of the eigenvalues of the one particle reduced density operator; in addition, from a variational argument concerning the ground state wave function, they give an estimation of the condensed fraction in superfluid helium four.

[3] Here, we discuss only homogeneous systems (a gas in a box), where translation invariance ensures that the number density n remains constant. When this symmetry is not fullfilled, as is the case in atomic traps, repulsive interactions have important secondary effects, in particular, the spatial density of the system is changed [24], with a significant decrease of the number density n of the atoms at the center of the trap (at constant total number of atoms); this reduces the degeneracy parameter $n\lambda^3$ at the center of the trap and, obviously, the transition temperature as well. Mean-field theories can be used to account qualitatively for the changes of spatial distributions of atomic gases in traps and, by the same token, for this change of critical temperature.
By contrast, the effects we are interested in in the present article are of a different nature; they originate from the microscopic correlations introduced between the particles by the interactions, so that they remain essentially beyond the scope of mean-field approaches. While the latter always predict that the transition occurs when $n\lambda^3$ is equal to 2.612.. at the point of maximum density (center of the trap), exactly as for an ideal gas, the purpose of our study is precisely to study the changes of this number under the effects of interactions; in other words, we are interested in changes of the critical value of the degeneracy parameter $n\lambda^3$, not in changes in n. Under these conditions, it is more convenient to assume that the gas is contained in a box, since then n automatically remains constant, so that the pure correlations effects are seen with no background due to density changes.

[4] One would expect the Hartree-Fock calculation to be better for dense systems, as all mean-field theories; in these systems each atom interacts simultaneously with many others, so that it can average most of its short range correlations with its neighbours, and experience only a mean field from them. Indeed, in a dense system such as superfluid helium 4, the basic prediction is the Hartree Fock calculation is borne out by experiments, since the critical temperature is found to be a decreasing function of pressure.
Nevertheless the domains of validity of the two methods should overlap at least partially (for a potential which would be at the same time weak and with short range) so that the prediction of what should happen in this case remains unclear.

a renormalization group calculation was given by Toyoda [29], which also predicted a decrease of the critical temperature; but subsequent more refined calculations by Stoof and coll. led to a prediction of an increase of the temperature [30,31]. The most recent result was obtained by a numerical calculation based on the path integral quantum Monte-Carlo method [32], and actually predicts the existence of a crossover between two regimes, at low and high densities; at low densities the critical temperature is indeed increased – but even in this region the results do not really agree with any of the analytical calculations mentioned above – see also reference [33] for another discussion of the low density regime. One can summarize the situation by saying that there is no known consensus on what is the expression of the second virial correction to the Bose-Einstein transition temperature in a dilute gas.

More generally, one can be interested in a better understanding of the correlation that are implied by superfluidity in a gas: on a microscopic scale, what kind of organization in both momentum and ordinary space is responsible for the occurrence of superfluidity? It is often considered that superfluidity is an inherently different physical phenomenon from Bose-Einstein condensation; but what is exactly the difference between the microscopic mechanisms that lead to each of these transitions, and to what extent should they always appear at the same time? Another related question is how the macroscopic wave function and its non-linear evolution [34,35] build up from individual correlated particles, in a dilute gas where atoms are free most of the time, collisions are binary and short, so that mean-field methods are not necessarily well suited? The hope is that the study of Bose-Einstein condensation in dilute gases, where more precise *ab initio* calculations should be feasible than in dense systems, will allow a better understanding of the original phenomena observed in superfluid systems, including the stability against dissipation, vortices, various modes of oscillation (second sound), etc.; for a general review of the many recent theoretical contributions in the subject, see reference [36].

In this article, we will focus ourselves on the study of the effects of binary interactions on the transition temperature, in an approach of the problem where the populations of various individual states are kept free to vary in any way; they may adapt to the interactions and become more and more different from a Bose-Einstein distribution when the temperature of a gas is progressively cooled down. For this purpose, we will use the method of Ursell operators, already discussed in previous articles [37], which is well adapted to a detailed treatment of binary short range correlations between particles due for instance to hard cores; for a preliminary report of the method, see [39]. Here, instead of calculating the partition function of the system as in previous work, we will find it more convenient to directly evaluate the one-particle density operator; it turns out that this is not only more direct physically, but also mathematically more convenient, mostly because the weights of the diagrams are much simpler than those in the partition function [40].

It is well-known [41–43] – and this was already emphasized in [39] in the context of Ursell operators – that, near the transition point, larger and larger exchange cycles of identical atoms become more and more important: infinite summations over many sizes of diagrams are therefore necessary. This task can be performed by using implicit integral equations; in a first step, we will use the simplest form for this equation, which is reminiscent of the Dyson equation, and this will lead us to a first form of the Ursell theory that is very similar to a mean-field theory. Not surprisingly then, we will find at this stage that the critical degeneracy parameter $n\lambda^3$ is unchanged, keeping exactly the same value as for an ideal gas; moreover, the velocity distribution of atoms will also remain the same as for an ideal gas, with of course some change of the effective chemical potential introduced by the interactions. This first step is to be seen mostly as a starting base where known results are recovered. The second step will involve a slightly more elaborate integral equation for the density operator, which fortunately is not much more complicated than the Ursell-Dyson equation so that it can be solved by a similar method. The major new feature introduced is a velocity dependence that is no longer that of an ideal gas: it includes a distortion of the velocity profile, especially at low velocities, a feature which is essentially beyond mean-field approximations. We will interpret this result as due to a spatial re-arrangement of atoms with low velocities, which allows them to minimize repulsion and, so to say, come closer to Bose-Einstein condensation than the other atoms. Consequently, the system has stronger tendency to populate lower states than it would have in the absence of interactions, which favors even more the ground state, so that it is still true that a single quantum state tends to be macroscopically populated; in a way, our reasoning can be seen as a more elaborate version of the argument concerning the role of interactions developed earlier by Nozières [19], as we discuss in more detail below. An important consequence of this effect is that the critical degeneracy parameter is reduced (still assuming repulsive interactions), by an amount which is compatible with the numerical Monte-Carlo results of reference [32]. More generally, this study provides a microscopic mechanism for the approach to Bose-Einstein condensation in a dilute gas.

Section 2 below is the most technical part of this article, with diagrams, counting, etc.; it can be skipped by the reader who is prepared to accept without justification the integral equations proposed in Section 3 for the one-particle density operator .

2 Ursell expansion of the one-body density operator

In [37] we have shown how a finite truncation of the Ursell operator series of the grand potential can provide virial corrections for quantum gases, even if they are partially degenerate; in [38] the same technique provided simple expressions for the one and two particle density operator.

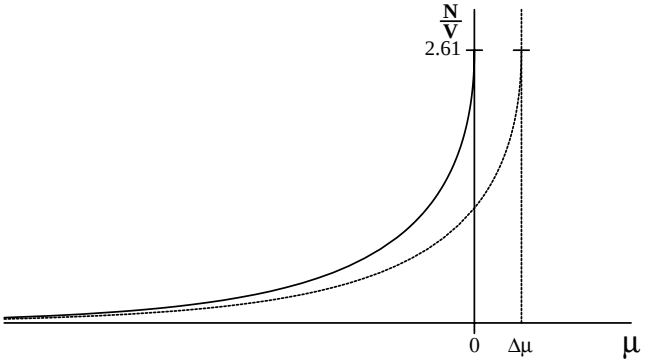

Fig. 1. Density of an ideal gas as a function of the chemical potential μ. If the effect of the interactions was simply to shift the critical value of μ by an amount $\Delta\mu$ (broken lines), a first order theory would provide a correction which diverges when μ tends to zero.

Nevertheless, in this article, we can not limit ourselves to these results, since they do not remain valid close to the Bose-Einstein condensation point. In fact any finite truncated expression, if taken seriously, would not give an acceptable description of the phase transition; in some cases, as discussed in Section 3.3 of reference [39], the transition would be replaced by a sharp but continuous crossover phenomenon, occurring over a finite range of parameters (which is independent of the size of the system but becomes narrower and narrower when the density of the gas decreases). But this conclusion arises from an incorrect simplification: it is clear that the validity of any truncation always ends up breaking down at some point when the system comes sufficiently close to Bose-Einstein condensation. Mathematically, the reason is that higher order terms in the series of perturbations, if they have smaller coefficients in a dilute system, also contain more denominators which diverge when the chemical potential tends to zero[5]; this implies stronger divergences near the transition point, so that higher order terms always become dominant at some point. Physically, the reason of this behavior is a divergence of the sizes of typical exchange cycles at the transition point [41,42].

Of course, observing divergences in perturbation series at a phase transition point is very common in physics. In the case of Bose-Einstein transition, nevertheless, an unusual feature is that the transition already exists in the ideal gas, and moreover already contains a strong singularity: the slope of the curve giving the density as a function of the chemical potential μ becomes infinite at the Bose Einstein critical point $\mu = 0$ (see Fig. 1).

This makes the problem more complicated. To see why, assume for a moment that the effect of the interactions is just to change this critical value by a small amount $\Delta\mu$, positive if the interactions are repulsive, negative if they are attractive. In this case, the behavior of the density near the critical value of μ would be given by:

$$n \simeq c_1 - c_2\sqrt{-(\mu + \Delta\mu)}. \tag{1}$$

This function can be expanded in a Taylor series of powers of $\Delta\mu$, and the result is a series where the term in $(\Delta\mu)^n$ is proportional to $1/|\mu|^{n-1/2}$ which, if μ tends towards zero (by negative values), diverges more and more strongly when its order increases; clearly the validity of the expansion breaks down at the transition point. This is a consequence of the non-analicity of the unperturbed function at the origin (an square root with an infinite derivative) while, despite of this mathematical problem, the physical nature of the transition would remain completely unaffected by the presence of a small correction $\Delta\mu$. This example illustrates the dangers of using finite perturbation series near a transition point[6]; this is why we have to go beyond the expressions written in [38] and to use a method where series are summed up to an infinite order.

2.1 Operatorial derivative

The Ursell diagrams that we will use in this article are similar to, but slightly different from those used in reference [37]: instead of the grand potential, what will be expanded here is the expression of the one-particle density operator. In any case, the two sorts of diagrams are closely related, since reduced density operators can be derived from the grand canonical partition function [38]. But, instead of first introducing the diagrams and then taking derivatives, it turns out to be more convenient to start again the calculation from the beginning, mostly because this avoids introducing weights that, in a second step, will be cancelled in many cases.

We use the same notation as in [37,38]; the P_α's are all the $N!$ permutations of the N particles, which will be expressed as products of permutation cycles; the U_n's are the Ursell operators. The first Ursell operator U_1 is defined as function of the one particle Hamiltonian H_1 (kinetic energy for a gas in a box) as:

$$U_1(1) = \exp\left[-\beta H_1(1)\right] \tag{2}$$

while the second operator U_2 is defined as a function of the two-particle Hamiltonian H_2 (including interactions between the two particles) by:

$$U_2(1,2) = \exp\left[-\beta H_2(1,2)\right] - \exp\left[-\beta H_1(1)\right]\exp\left[-\beta H_1(2)\right] \tag{3}$$

(similar expressions can be written for the higher rank Ursell operators). Equation (9) of reference [37] provides

[5] In Ursell diagrams, every horizontal line introduces, after a summation over the size of the cycles, a factor $(1+f_1)$ (where f_1 is the one particle distribution of the ideal gas) which diverges when $\mu \to 0$. Therefore, the more lines the diagram contains, the more divergent it is.

[6] It is not necessarily realistic: in fact we will see in this article that the effects of interactions are more interesting than a simple shift of the value of the chemical potential. It is nevertheless interesting to note that several of the properties that we will find in our more elaborate study depend critically on the singularity of the curve giving the density of an ideal gas.

the following expression of the N particle partition function:

$$Z_N = \frac{1}{N!} \sum_{\{P_\alpha\}} \sum_{\{U\}} \prod_{\text{clusters}} \Gamma_{\text{cluster}}(i,j,k...) \tag{4}$$

where each of the $\sum$ in equation (4) is actually a simplified notation for two different summations; the sum over $\{U\}$ is meant to contain a sum over all possible ways to write products of U_n's containing altogether N particles[7], as well as another sum over all possible non-equivalent ways to put numbered particles into these U's – see equation (4) of [37]; similarly, the sum over $\{P_\alpha\}$ is meant to contain all possible ways to write products of cycles for N particles[8] as well as all non-equivalent ways to distribute numbered particles in them – see Section 2 of [37] for more details. The $\Gamma(i,j,k...)$ are the "explicit" expressions of the clusters, in fact traces involving numbered particles $(i,j,k...)$ which are grouped together into the same cluster by either Ursell operators or permutation cycles.

To obtain the one-particle density operator, it is convenient to set (for $n \geq 2$):

$$U_n(1,2,..n) = \overline{U}_n(1,2,..n) \times U_1(1) \times U_1(2) \times ...U_1(n) \tag{5}$$

where all the $\overline{U}_n$ will be kept constant, while the operators U_1's will be varied according to:

$$\mathrm{d}U_1 = \mathrm{d}x \times U_1|\varphi\rangle\langle\theta|. \tag{6}$$

Here the kets $|\varphi\rangle$ and $|\theta\rangle$ are any kets in the one-particle state space. As shown in [38], the one-particle density operator $\rho_1^{(N)}$ in the canonical ensemble is then given by:

$$\langle\theta|\rho_1^{(N)}|\varphi\rangle = \frac{1}{Z_N}\frac{\mathrm{d}}{\mathrm{d}x} Z_N. \tag{7}$$

In each term of the double sum in (4), one has to take the derivatives of all Γ's with respect to x in succession, which amounts to taking the derivative with respect to the U_1 operator of every numbered particle. The diagram which contains the particle in question then becomes an operator $\widehat{\Gamma}_{\text{cluster}}(i,j,k)$, so that we obtain the expression:

$$\rho_1^{(N)} = \frac{1}{N! Z_N} \sum_{i=1}^{N} \sum_{\{P_\alpha\}} \sum_{\{U\}} \widehat{\Gamma}_{\text{cluster}}(i,j,k) \times \prod_{\text{rest}} \Gamma_{\text{cluster}}(m,p,q...) \tag{8}$$

where $\prod_{\text{rest}}$ symbolizes the product over all remaining Γ_{cluster}'s which have not be modified by the derivative; sometimes, we will call this expression "the triple sum".

[7] This summation corresponds to the sum over the m_l''s in equation (4) of [37].

[8] This summation corresponds to the sum over the m_i's in equation (7) of [37].

Fig. 2. An example of an $U - C$ term in the expansion of the partition function Z.

2.2 An example

As an example, let us for instance take the following cluster, corresponding to the diagram shown in Figure 2:

$$\Gamma(1,2,..8) = \mathrm{Tr}_{1,2,...8}\left\{\overline{U}_2(1,7)U_1(1)U_1(2).....U_1(7)U_1(8)C_6(1,..6)C_2(7,8)\right\} \tag{9}$$

where the C's are the permutation cycles - $C_6(1,..6)$ is the operator which creates a circular permutation of particles 1, 2, ...6 while $C_2(7,8)$ is merely the exchange operator for particles (7) and (8). Assume for instance that we take the derivative with respect of particle $i = 4$; we then have to evaluate the following expression:

$$\mathrm{Tr}_{1,2,...8}\{\overline{U}_2(1,7)U_1(1)U_1(2) ...\widetilde{U}_1(4)U_1(5)..U_1(7)U_1(8)C_6(1,..6)C_2(7,8)\} \tag{10}$$

with the notation:

$$\widetilde{U}_1 = U_1|\varphi\rangle\langle\theta|. \tag{11}$$

Expression (10) is nothing but the matrix element:

$$\langle\theta|\widehat{\Gamma}_{\text{cluster}}(1,2,..8)|\varphi\rangle \tag{12}$$

which can be obtained calculated by the same method of calculation as in [37], with the introduction of a sufficient number of closure relations $\sum_n |u_n\rangle\langle u_n|$ in one-particle spaces. In this way, one gets the expression:

$$\sum_{n_1,.....,n_8} \langle 1:u_{n_1}|\langle 2:u_{n_2}|... ...\langle 8:u_{n_8}|\overline{U}_2(1,7)U_1(1)U_1(2) \times ....\widetilde{U}_1(4) \times U_1(5)..U_1(7)U_1(8)|1:u_{n_2}\rangle|2:u_{n_3}\rangle \times ...|5:u_{n_6}\rangle|6:u_{n_1}\rangle|7:u_{n_8}\rangle|8:u_{n_7}\rangle. \tag{13}$$

Considering first particles 1, we see that the circular permutation of indices in the kets at then end of the expression, together with the summation over indices n_2, n_3,...n_6, introduce the product of operators:

$$\overline{U}_2(1,7)\left[U_1(1)\right]^3 \widetilde{U}_1(1)\left[U_1(1)\right]^2 \tag{14}$$

while the summation over n_1 introduces a trace over particle 1; similarly, the summation over n_8 introduces the product of two additional operators $U_1(7)$. Finally we get:

$$\mathrm{Tr}_{1,7}\left\{\overline{U}_2(1,7)\left[U_1(1)\right]^3 \widetilde{U}_1(1)\left[U_1(1)\right]^2\left[U_1(7)\right]^2\right\}, \tag{15}$$

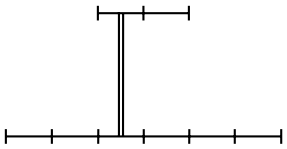

Fig. 3. An example of an $U - C$ term in the expansion of the one-particle density-operator ρ_1.

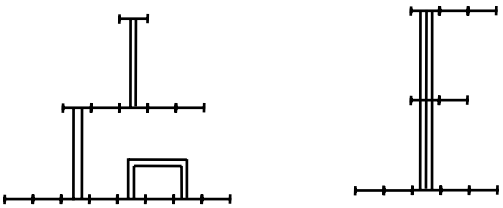

Fig. 4. Two examples of diagrams occurring in the expansion of ρ_1; the diagram on the left has a weight 1, but that on the right has a weight 1/2.

which is nothing but the matrix element (the dummy index (7) is renamed into (2)):

$$\langle 1:\theta|\mathrm{Tr}_2\left\{[U_1(1)]^2 \times [U_1(2)]^2\,\overline{U}_2(1,2)\,[U_1(1)]^3\,U_1(1)\right\}|1:\varphi\rangle. \quad (16)$$

Finally we obtain:

$$\widehat{\Gamma}_{\mathrm{cluster}}(1,2,..8) = \mathrm{Tr}_2\left\{[U_1(1)]^2\,\overline{U}_2(1,2)\,[U_1(1)]^4\,[U_1(2)]^2\right\} = [U_1(1)]^2\,\mathrm{Tr}_2\left\{U_2(1,2)U_1(2)\right\}[U_1(1)]^3. \quad (17)$$

This is, of course, an operator – no longer a number as was the initial Γ; but it can also be represented by a diagram, such as that shown in Figure 3. In this new diagram, the lowest horizontal line no longer corresponds to a trace but to a product of operators $U_1(1)$ – as many as there are segments in this line (two in this particular case) – interrupted at some point by a $U_2(1,2)$, and then followed by another horizontal line symbolizing again the product of U_1's (three in this case). On the other hand, the upper horizontal line still corresponds to a trace over particle 2; it also contains operators $U_1(2)$, but here they all remain after the operator $U_2(1,2)$.

2.3 Diagrams; weights

More generally, all operators $\widehat{\Gamma}$ in the triple sum (8) can be represented by diagrams where the lowest horizontal line represents a product of operators, beginning by either a chain of U_1's, or a single U_1, or actually any U_n; this is the main difference with diagrams contained in Z (or $\log Z$), where the initial operator was always that of highest rank. All the other horizontal lines correspond to traces, and begin necessarily with an operator or rank at least $n = 2$; in fact, these lines behave exactly as those in $\log Z$. In other words the new diagrams are, so to say, obtained by "cutting", or "opening" the old diagrams at some arbitrary point, taken in some exchange cycle[9], which then no longer corresponds to a trace but to a product of operators – see the two examples shown in Figure 4.

As in [37], we need a rule to decide precisely how the diagrams should be drawn; this is necessary in order to avoid ambiguities and double counting. Fortunately, the fact that the derivative has "tagged" one particle – adding one summation to the two which already exist in (4) – makes the problem much simpler. The tagged particle determines the first operator of the lowest exchange cycle; it provides a well defined starting point, a "root" from which one can propagate horizontally along exchange cycles and vertically along U_2's or operators of higher rank. Actually, when only U_2 operators are present in the diagram, no ambiguity ever occurs: the simple propagation from the root into the branches is sufficient to assign a well defined structure to each term – see for instance the first example of Figure 4. Only when operators U_n of rank n equal to 3 (or more) occur, as in the second example of this figure, can some ambiguity occur: which is cycle is in the middle, which one in the upper position? By similarity with what was done in [37], we take the following convention: beyond the first particle, which is determined by propagation along a previous cycle, all the other particles in U_n's of rank equal to 3 (or more) appear in order of increasing numbering; in other words, in the vertical lines, particles appear with an upward increasing numbering, except of course for the lowest particle which is either the tagged particle, or is determined from it by propagation along previous cycles and U_n's. With this rule combined with those of [37], each contribution to $\rho_1^{(N)}$ appearing in the triple sum (8) corresponds to a perfectly well defined series of diagrams, starting with an operator $\widehat{\Gamma}_\rho$, and followed by a product of numbers $\Gamma_{\mathrm{diag.}}$.

Conversely, if we did not specify any numbering in the diagrams, it is clear that the same series of diagrams corresponds to many different terms in the triple sum (8)[10]; in order to get a one-to-one correspondence, we have to specify particle numbers at each location inside the diagrams, in other words to consider "numbered diagrams" where each "site" in the diagrams gets a number. This can be done precisely by the rules mentioned in the preceding paragraph: starting from the tagged particle in $\widehat{\Gamma}_\rho$, one adds horizontally the particles it exchanges with (in the order of the cyclic permutation), and then progresses vertically along higher order rank U_n's: this provides a unique distribution of all relevant particles – as for the $\Gamma_{\mathrm{diag.}}$'s, they are of course treated exactly as in [37]. We can

[9] This cycle may of course be of length one, corresponding to no exchange at all.

[10] In fact, a given $\widehat{\Gamma}_\rho$ may even originate from several different $\Gamma_{\mathrm{diag.}}$'s; but this is no longer true as soon as it contains numbered sites (the lowest of all numbers in the U_n of highest rank will determine the root of the $\widehat{\Gamma}_\rho$).

then write:

$$\rho_1^{(N)} = \frac{1}{N! Z_N} \sum_{\text{diag.}} \sum_{\text{distrib.}} \widehat{\Gamma}_\rho(\,.\,,\,.\,,\,.\,) \prod_{\text{rest}} \Gamma_{\text{diag.}}(\,.\,,\,.\,,\,.\,) \tag{18}$$

where $\sum_{\text{diag.}}$ stands for all the possible ways to write series of diagrams, one Γ_ρ and one arbitrary number of $\Gamma_{\text{diag.}}$'s, for a total number of particles equal to N; in addition, $\sum_{\text{distrib.}}$ introduces a summation over all correct ways to distribute numbered particles into the series. One should keep in mind that any random distribution of numberings in a diagram $\widehat{\Gamma}_\rho$ is not necessarily acceptable: in general; in fact, only a proportion g_ρ is correct (similarly, only a proportion $f_{\text{diag.}}$ is acceptable for diagrams $\Gamma_{\text{diag.}}$, as discussed in [37]). We call this proportion the weight of the diagram; for instance, if a diagram contains one U_3, the value of g_ρ is $1/2$; if it contains p operators U_3's its value is $1/2^p$; if it contains q operators U_4, its value is $1/6^q$, etc.

2.4 Counting diagrams

It is now possible to get rid of particle numbering which, of course, does not affect the contribution to ρ_1 of any particular term. Let us choose one given (non-numbered) diagram Γ_ρ, call n_ρ the number of particles it contains, and calculate the total coefficient that it gets from the summations of (18):

$$\frac{1}{N!} \sum_{\text{distrib.}} \widehat{\Gamma}_\rho(.,.,.) \sum_{\text{diag. rest}} \prod \Gamma_{\text{diag.}}(.,.,.,). \tag{19}$$

This can be done in two steps: first calculate the contribution of the term $\Gamma_\rho(i,j,k)$ when the particles (i,j,k) are a given sub-ensemble of the N particles; then sum over all the ways to select this sub-ensemble. The first step can be made by remarking that, for the $N - n_\rho$ remaining particles, the $\sum_{\text{distrib.}}$ can be moved to the right of Γ_ρ , which introduces the same expression as in [37]; therefore the summation of the products of $\Gamma_{\text{diag.}}$'s merely reconstructs the partition function Z_{N-n_ρ} of $N - n_\rho$ particles, multiplied by $(N - n_\rho)!$. As for the n_ρ particles, one has to take into account the number of correct distributions of the n_ρ particles in the first diagram, which is $(n_\rho)! g_\rho$. For the second step, we first have to multiply the result by the number of ways to distribute n_ρ particles among N, which is:

$$\frac{N!}{(N-n_\rho)!(n_\rho)!}\,. \tag{20}$$

Taking all these factors into account, we obtain the following result:

$$\frac{1}{N! Z_N} \frac{N!}{(N-n_\rho)!(n_\rho)!} (n_\rho)!\; g_\rho \times (N-n_\rho)!\; Z_{N-n_\rho} \times \widehat{\Gamma}_\rho \tag{21}$$

so that our final expression for the canonical ensemble is:

$$\rho_1^{(N)} = \sum_{\rho \text{ diagrams}} \frac{Z_{N-n_\rho}}{Z_N} g_\rho \widehat{\Gamma}_\rho. \tag{22}$$

At this point, it becomes convenient to introduce the grand canonical ensemble and its partition function:

$$Z_{\text{g.c.}} = \sum_N z^N Z_N \tag{23}$$

where $z = \mathrm{e}^{\beta\mu}$ is, with usual notation, the fugacity; the corresponding one-particle density operator ρ_1 (to simplify the notation, we now give up the index g.c.):

$$\begin{aligned} \langle\theta|\rho_1|\varphi\rangle &= \frac{1}{Z_{\text{g.c.}}} \frac{\mathrm{d}}{\mathrm{d}x} Z_{\text{g.c.}} \\ &= \frac{1}{Z_{\text{g.c.}}} \sum_N z^N Z_N \langle\theta|\rho_I^{(N)}|\varphi\rangle. \end{aligned} \tag{24}$$

We then get:

$$\begin{aligned} \rho_1 &= \frac{1}{Z_{\text{g.c.}}} \sum_N z^N Z_N \sum_{\rho \text{ diagrams}} g_\rho \frac{Z_{N-n_\rho}}{Z_N} \widehat{\Gamma}_\rho \\ &= \frac{1}{Z_{\text{g.c.}}} \sum_{\rho \text{ diagrams}} z^{n_\rho} g_\rho \widehat{\Gamma}_\rho \sum_{N-n_\rho} z^{N-n_\rho} Z_{N-n_\rho}. \end{aligned} \tag{25}$$

But the second summation reconstructs is just another expression of the grand canonical partition function, so that we finally obtain:

$$\rho_1 = \sum_{\rho \text{ diagrams}} z^{n_\rho} g_\rho \widehat{\Gamma}_\rho. \tag{26}$$

This expression shows that the one-particle density operator is merely the sum of all diagrams $\widehat{\Gamma}_\rho$, with coefficients which are the product of the weight g_ρ by the fugacity raised to a power which is the number of particles contained in the diagram.

The simplest case is, of course, the ideal gas, for which the only diagrams are horizontal lines; we immediately get:

$$\rho_1 = \sum_{n=1}^{\infty} z^n \,[U_1]^n = f_1 \tag{27}$$

where f_1 is defined as usual by:

$$f_1 = \frac{zU_1}{1 - zU_1}\,. \tag{28}$$

Actually, even for interacting gases, this operator plays a role in the diagrams, or more precisely the sum:

$$\sum_{n=0}^{\infty} z^n \,[U_1]^n = 1 + f_1 \tag{29}$$

which can be connected for instance after any operator U_2. We take the same convention as in [37]: dashed horizontal lines symbolize this operator; the operator f_1 itself

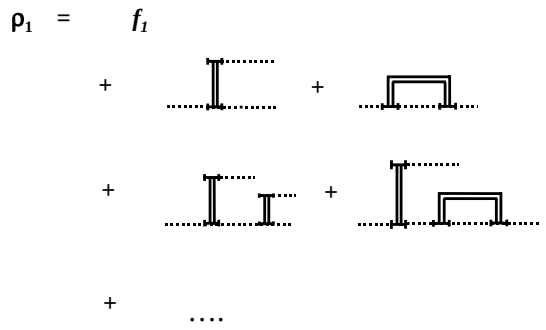

Fig. 5. The lowest order terms in the U-C expansion of the one-particle density-operator ρ.

is then represented by a dashed line connected to a one-case horizontal line ($f_1 = zU_1 + [1 + f_1]$). The first terms in the Ursell expansion of ρ_I are shown in Figure 5; those explicitly shown in the first and second line correspond to the "generalized Beth-Uhlenbeck approximation discussed in this reference, which in terms of ρ_1 would lead to the expression:

$$\rho_1 = f_1 + 2z^2\,[1 + f_1(1)] \times \mathrm{Tr}_2\left\{U_2^S(1,2)\,[1 + f_1(2)]\right\}[1 + f_1(1)]\,. \qquad (30)$$

A diagram where the same U_2 re-connects to the same cycle corresponds to an exchange term, where U_2 is replaced by its product by the exchange operator $P_{\mathrm{ex.}}$, as discussed in [37]; for instance, in the second line of Figure 5, the second diagram is merely the exchange term of the first.

3 Integral equations

The largest eigenvalue of U_1 corresponds to the ground state of the one-particle Hamiltonian H_1. When the chemical potential reaches the energy of this state (zero for a gas in a box with periodic boundary conditions), the action of each operator zU_1 leaves the ground state unchanged; then, the series of this operator which is contained in f_1 (sum of all of its powers) diverges. This is not surprising since, as already mentioned, Bose-Einstein condensation corresponds to a situation where the size of typical exchange cycles is no longer limited to a few units, but increases to infinity. For an interacting system, the phenomenon is not limited to chains of U_1's only: when very long exchange cycles become important, it is expected that typical diagrams will also contain an arbitrary large number of operators U_2 (or higher rank Ursell operators) connecting these cycles. In practice, this means that it is not possible to limit the calculations to a few diagrams, those shown explicitly in Figure 5 for instance; a summation over large categories of diagrams is indispensable.

This is what is done in the two sections below, first within a simplified approach which is useful as a preliminary step (it will lead us to a mean-field like theory), second within a more elaborate treatment.

3.1 A first approach: Dyson-Ursell equation

For simplicity, we limit ourselves for the moment to terms which contain Ursell operators of rank 1 and 2, while a generalization to higher ranks is possible in a similar way. The symmetrized version of U_2 is:

$$U_2^S = \frac{1}{2}\,[1 + P_{\mathrm{ex.}}]\,U_2 = \frac{1}{2}U_2\,[1 + P_{\mathrm{ex.}}] \qquad (31)$$

where $P_{\mathrm{ex.}}$ is the exchange operator of the two particles contained in U_2 (we only study bosons here); the factor $1/2$ in front of this definition is introduced for the first part of the formula to be a projector (if necessary, one can put projectors on each side of U_2 without changing the result).

Let us now write the following implicit equation:

$$\rho_1(1) = f_1(1) + 2z^2\,[1 + f_1(1)] \times \mathrm{Tr}_2\left\{U_2^S(1,2)\,[1 + \rho_1(1)]\,[1 + \rho_1(2)]\right\} \qquad (32)$$

and investigate which diagrams are contained in it. The zero order term in U_2 is merely f_1; the first order terms in U_2 are simply the second and the third diagram of Figure 5 – in [37] we showed how terms introduced by the exchange operator correspond to diagrams where the same U_2 touches twice the same horizontal exchange cycle. More generally, it is easy to see that the term $\rho_1^{(n)}$ of order n in U_2 is obtained as a function of terms of lower order by the relation[11]:

$$\rho_1^{(n)} = 2z^2\,[1 + f_1(1)]\,\mathrm{Tr}_2\left\{U_2^S\,[1 + f_1(1)]\,\rho_1^{(n-1)}(2) + U_2^S\rho_1^{(1)}(1)\rho_1^{(n-2)}(2) + \ldots\ldots + U_2^S\rho_1^{(n-1)}(1)\,[1 + f_1(2)]\right\}. \qquad (33)$$

In the right hand side, let us first consider the direct term, where U_2^S is replaced by U_2: diagrammatically, in the two horizontal lines which follow U_2, one gets in succession all possible combinations of lower order "branches". For instance, two second order terms ($n = 2$) are shown in the third line of Figure 5; two others should follow with an additional U_2 connected in two different ways to the upper cycle. As for the exchange term, it gives a diagram where the first U_2 reconnects to the initial exchange cycle, so that this time it is the line between the two contact points and the line after the second point which play the role of the two lines after the U_2; nevertheless the situation remains essentially the same with a different topology (taking again the example of second order terms, one would get 4 more diagrams where the first U_2 is folded over the same initial cycle). We then see that, when the iteration is continued to infinity, it provides once, and once only, all possible "branched" diagrams with an arbitrary number of U_2's: indeed, equation (33) provides a convenient way

[11] The equation is written for the case where $n > 1$; if $n = 1$, the curly bracket of (33) is simply equal to $\left\{U_2^S\,[1 + f_1(1)]\,[1 + f_1(2)]\right\}$. A more precise discussion is given in Appendix A.

Fig. 6. Diagrams containing loops which are not included in the Ursell-Dyson approximation, but will be in the more elaborate integral equation of Section 3.2; the second diagram corresponds to the exchange term of the first.

to perform a summation containing an infinite number of diagrams and cycles with infinite length. Nevertheless one should keep in mind that this is not exact either: more complicated diagrams, which are not simply "branched", are still not included, for instance those containing loops such as those of Figure 6.

Remark: equation (32) is a simple generalization of (30), but one could think of other simple iteration equations[12], for instance:

$$\rho_1(1) = f_1(1) + 2z^2\,[1+\rho_1(1)] \times \mathrm{Tr}_2\left\{U_2^{S,A}(1,2)\,[1+\rho_1(1)]\,[1+\rho_1(2)]\right\} \quad (34)$$

(the only difference with (32) is that one f_1 has been replaced by one ρ_1). Nevertheless, one can easily convince oneself that this equation is not satisfactory since it just introduces redundancy, actually already at second order in U_2.

3.2 A more elaborate integral equation

The approximation made in the preceding section can be completed by adding terms where U_2 operators connect twice the same pair of cycles so that they introduce loops. In fact, to include them, it is sufficient to add the following term to the right hand side of (32):

$$z^4\,[1+f_1(1)] \times \mathrm{Tr}_2\left\{[U_2(1,2)\,[1+\rho_1(1)]\,[1+\rho_1(2)]]^2\,[1+P_{\mathrm{ex.}}]\right\} = 2z^4\,[1+f_1(1)]\,\mathrm{Tr}_2\left\{\left[U_2^S(1,2)\,[1+\rho_1(1)]\,[1+\rho_1(2)]\right]^2\right\} \quad (35)$$

(the second line is easily obtained by introducing the symmetrizer $[1+P_{\mathrm{ex.}}]/2$, which is a projector and can therefore be raised to any power, and using the commutation between this operator and U_2). When this is done, diagrams with an arbitrary number of pairs of U_2's touching twice the same two cycles are included, as illustrated by the example shown in Figure 7. Note that, since the right hand side of equation (33) now contains the sum of two terms, any combination remains possible: some cycles may be connected only once by a U_2, others twice. We note in passing that, in these new diagrams, every U_2 does not necessarily introduce a trace over a new particle, as opposed to the situation in branched diagrams.

[12] Another remark is that the 1's are indispensable in (32); otherwise diagrams where U_2 is not directly followed with U_1''s would be excluded.

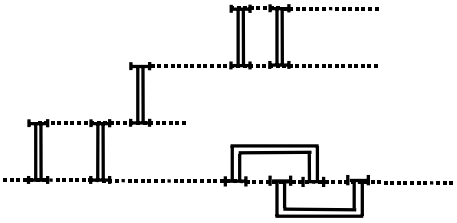

Fig. 7. A typical diagram containing several loops, which is included in equation (37).

There is no special difficulty in including now terms with an arbitrary number q of operators U_2's forming a ladder between the same two cycles; one now has to add the following term to the right hand side of (33):

$$z^{2q}\,[1+f_1(1)] \times \mathrm{Tr}_2\left\{[U_2(1,2)\,[1+\rho_1(1)]\,[1+\rho_1(2)]]^q\,[1+P_{\mathrm{ex.}}]\right\} = 2z^{2q}\,[1+f_1(1)]\,\mathrm{Tr}_2\left\{\left[U_2^S(1,2)\,[1+\rho_1(1)]\,[1+\rho_1(2)]\right]^q\right\}. \quad (36)$$

The summation of all these contributions, from $q=1$ as in Section 3.1 up to infinity, is possible and provides the following generalization of (32):

$$\rho_1(1) = f_1(1) + 2z^2\,[1+f_1(1)] \times \mathrm{Tr}_2\left\{\frac{U_2^S(1,2)\,[1+\rho_1(1)]\,[1+\rho_1(2)]}{1-z^2U_2^S(1,2)\,[1+\rho_1(1)]\,[1+\rho_1(2)]}\right\}. \quad (37)$$

At this level of approximation, diagrams similar to that of Figure 7 with a completely arbitrary number of vertical lines connecting the same two cycles are generated. It is interesting to note that the summation of diagrams introduces into the trace an operator which can be seen as a two body generalization of the one particle distribution function of the ideal gas; one can easily see that more complex terms would introduce three particle terms, etc.

3.3 Discussion

Clearly, the fact that almost all weights are eliminated from the diagrams for the density operator (if no other operator than U_1 and U_2 is considered) is the source of great simplification in all calculations; similar calculations for the expansion of $\log Z$ would have been much more difficult. If necessary, one could readily include in the integral equation more complicated terms, such as for instance that corresponding to the diagrams of Figure 8, or the second diagram of Figure 4, chained an arbitrary number of times. We will see, nevertheless, that in dilute gases only a limited ensemble of diagrams play a role in the determination of the critical temperature.

Fig. 8. Examples of diagrams that are not included in equation (37).

4 A mean-field like approximation

We first study equation (32) and calculate the value of the diagonal elements $\rho_{\mathbf{k}}$ of the one-particle density operator; translational invariance in a box with periodic boundary conditions ensures that the plane waves $|\mathbf{k}\rangle$ are the eigenstates of ρ_1. These diagonal elements are then:

$$\rho_{\mathbf{k}} = \langle \mathbf{k}|\rho_1|\mathbf{k}\rangle \tag{38}$$

while, for the ideal gas, they have the value:

$$f_{\mathbf{k}} = \langle \mathbf{k}|f_1|\mathbf{k}\rangle = \frac{\mathrm{e}^{-\beta\widetilde{e}_k}}{1-\mathrm{e}^{-\beta\widetilde{e}_k}} = \frac{1}{\mathrm{e}^{\beta\widetilde{e}_k}-1} \tag{39}$$

where f_1 has been defined in (28) and $\widetilde{e}_k$ is the difference between the energy and the chemical potential:

$$\widetilde{e}_k = e_k - \mu = \frac{\hbar^2 k^2}{2m} - \mu \tag{40}$$

and m the mass of the bosons. We will also replace the value of the diagonal matrix elements of U_2^S by their expression as a function of the (symmetrized) Ursell length $a_U^S(k)$, which is given in equations (17, 4) of [45]:

$$z^2\langle \mathbf{k},\mathbf{k}'|U_2^S|\mathbf{k},\mathbf{k}'\rangle = -\frac{\lambda_T^2}{\mathcal{V}}\mathrm{e}^{-\beta[\widetilde{e}_k+\widetilde{e}_{k'}]} \times a_U^S(|\mathbf{k}-\mathbf{k}'|) \tag{41}$$

where λ_T is the thermal wavelength:

$$\lambda_T = \frac{h}{\sqrt{2\pi m k_{\mathrm{B}} T}} \tag{42}$$

(with usual notation) and $\mathcal{V}$ the volume of the container. But, as shown in this reference, the symmetric Ursell length is almost constant at low energies and equal to twice[13] the scattering length a (if interactions occur *via* hard cores, a is merely their diameter). We therefore write:

$$z^2\langle \mathbf{k},\mathbf{k}'|U_2^S|\mathbf{k},\mathbf{k}'\rangle = -2\frac{\lambda_T^2}{\mathcal{V}}\mathrm{e}^{-\beta[\widetilde{e}_k+\widetilde{e}_{k'}]} \times a \tag{43}$$

which is a very good approximation for low temperature gases (except, of course, if accidental collision resonances occur at very low energies); moreover we will assume in all the rest of this article that a is positive (repulsive interactions).

[13] This factor two corresponds to the well-known statistical increase of the interaction between two identical bosons.

4.1 A set of non-linear coupled equations

Projecting (32) over the plane waves provides the relation:

$$\rho_{\mathbf{k}} = f_{\mathbf{k}} + \sum_{\mathbf{k}'}[1+f_{\mathbf{k}}]\left[-\frac{4a\lambda_T^2}{\mathcal{V}}\right] \times \mathrm{e}^{-\beta[\widetilde{e}_k+\widetilde{e}_{k'}]}[1+\rho_{\mathbf{k}}][1+\rho_{\mathbf{k}'}]. \tag{44}$$

It is convenient to introduce the variables:

$$X_{\mathbf{k}} = \mathrm{e}^{-\beta\widetilde{e}_k}[1+\rho_{\mathbf{k}}] \tag{45}$$

as well as the dimensionless coupling constant:

$$\alpha = 4\frac{\lambda_T^2}{\mathcal{V}}a. \tag{46}$$

Dividing both sides of equation (44) by the same factor $[1+f_{\mathbf{k}}]$ then provides the simpler equation:

$$\alpha\sum_{\mathbf{k}'}X_{\mathbf{k}'}X_{\mathbf{k}} - \xi_k X_{\mathbf{k}} - 1 = 0 \tag{47}$$

with the notation:

$$\xi_k = 1 - \mathrm{e}^{\beta\widetilde{e}_k}. \tag{48}$$

These equations can be obtained by stationarity conditions applied to a function Φ; see Appendix B.

If all variables $X_{\mathbf{k}'}$ except $X_{\mathbf{k}}$ are considered as given, $X_{\mathbf{k}}$ is the solution of a simple quadratic equation:

$$\alpha(X_{\mathbf{k}})^2 - \xi_k^{'}X_{\mathbf{k}} - 1 = 0 \tag{49}$$

with:

$$\xi_k^{'} = \xi_k - \Delta\overline{\xi}_k \tag{50}$$

and[14]:

$$\Delta\overline{\xi}_k = \alpha\sum_{\mathbf{k}'\neq\mathbf{k}}X_{\mathbf{k}'}. \tag{51}$$

The solution is straightforward:

$$X_{\mathbf{k}} = \frac{1}{2\alpha}\left[\xi_k^{'} + \sqrt{\left(\xi_k^{'}\right)^2+4\alpha}\right] \tag{52}$$

but one should keep in mind that this is an implicit solution: $X_{\mathbf{k}}$ depends on all the other $X_{\mathbf{k}'}$ through $\Delta\overline{\xi}_k$ (which accounts for the mean repulsion exerted by all the other levels), while in turn these variables depend on $X_{\mathbf{k}}$ through their own $\Delta\overline{\xi}_{k'}$. The corresponding system of coupled equations will be solved graphically in the next section; for the moment, we assume for simplicity that all $X_{\mathbf{k}'}$'s are kept constant and study the variations of $X_{\mathbf{k}}$.

[14] The bar in $\Delta\overline{\xi}$ is used to emphasize the mean-field character of this correction; in the next section we will include in $\xi_k^{'}$ additional terms arising from correlations.

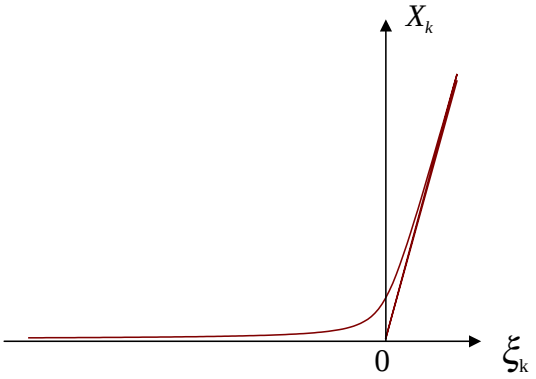

Fig. 9. Variations of X_k as a function of ξ_k; when ξ_k is positive, X_k reaches a regime where it becomes proportional to the volume of the system.

Figure 9 shows this variations as a function of $\xi_k^{'}$. We can distinguish between two different regimes; first, when $\xi_k^{'}$ is negative, one gets from (52):

$$X_{\mathbf{k}} \simeq -\frac{1}{\xi_k'} = \frac{1}{\mathrm{e}^{\beta\widetilde{e}_k} - 1 + \Delta\overline{\xi}_k} \tag{53}$$

and:

$$\rho_{\mathbf{k}} = \mathrm{e}^{\beta\widetilde{e}_k} X_{\mathbf{k}} - 1 = \frac{1 - \Delta\overline{\xi}_k}{\mathrm{e}^{\beta\widetilde{e}_k} - 1 + \Delta\overline{\xi}_k} \tag{54}$$

which is very reminiscent of the equations for the ideal gas; for instance, if $\beta\widetilde{e}_k \ll -1$, the population of the level in question is given by a Boltzmann exponential. Actually, the effect of the "mean repulsion" $\Delta\overline{\xi}_k$ can be expressed in terms of a positive correction to the chemical potential:

$$\Delta\overline{\mu}_k = -\beta^{-1}\log\left(1 - \Delta\overline{\xi}_k\right) \tag{55}$$

so that, with this notation, (54) becomes:

$$\rho_{\mathbf{k}} = \frac{1}{\mathrm{e}^{\beta\widetilde{e}_k + \Delta\overline{\mu}_k} - 1} = f_1(k; \mu - \Delta\overline{\mu}_k). \tag{56}$$

The second regime occurs when $\xi_k^{'}$ crosses zero and becomes positive: in this process, the population does not diverge, in contrast to what would happen for the ideal gas, but reaches a new regime where its value depends explicitly of the coupling constant:

$$X_{\mathbf{k}} \simeq \frac{\xi_k^{'}}{\alpha}\,. \tag{57}$$

Actually, since α is inversely proportional to the volume, the population in question becomes extensive, as expected for the ground state when it undergoes Bose-Einstein condensation.

Equations (51, 53) provide the system of coupled equations to be solved: each $X_{\mathbf{k}}$ depends on the value of its associated $\Delta\overline{\xi}_k$, which in turn depends on all the other $X_{\mathbf{k}'}$'s; in general, the solution is complicated. Fortunately, in the thermodynamic limit, it becomes simpler since the contribution of each single $X_{\mathbf{k}'}$ to $\Delta\overline{\xi}_k$ becomes negligible, so that the sum in (51) can be extended to include $\mathbf{k}^{'} = \mathbf{k}$ and become independent of $\mathbf{k}$. This is because, as shown by definition (46), the coupling constant α tends to zero when the volume becomes infinite, while the correction $\Delta\overline{\xi}_k$ remains finite (in the same limit, the discrete sum becomes an integral which contains a density of states which is proportional to the volume). In fact, for the contribution of a single $X_{\mathbf{k}'}$ to remain significant, the level in question has to get a population which is proportional to the volume (extensive).

In what follows we will therefore replace all the $\Delta\overline{\xi}_k$'s by the same value $\Delta\overline{\xi}$ defined by:

$$\Delta\overline{\xi} = \alpha\sum_{\mathbf{k}} X_{\mathbf{k}} = \frac{\alpha\mathcal{V}}{8\pi^3}\int \mathrm{d}^3\mathbf{k}\; X(\mathbf{k}). \tag{58}$$

This is possible as long as the system is not Bose condensed; but, if one level $\mathbf{k}_0$ were condensed, one would have to add its contribution $\alpha X_{\mathbf{k}_0}$ to this integral.

4.2 Graphical solution

We can solve the coupled equations by a self-consistent procedure: first we consider $\Delta\overline{\xi}$ as given, then use its value to calculate the $X_{\mathbf{k}}$'s, from which we can obtain the sum (we assume that the system is not condensed):

$$\frac{\alpha\mathcal{V}}{8\pi^3}\int \mathrm{d}^3\mathbf{k}\; X(\mathbf{k}) = 4\frac{a}{\lambda_T} J(\Delta\overline{\xi}) \tag{59}$$

where J is the dimensionless integral:

$$J = \left(\frac{\lambda_T}{2\pi}\right)^3 \int \mathrm{d}^3\mathbf{k}\; X(\mathbf{k}). \tag{60}$$

Finally, we close the system by writing that the integral (59) is nothing but $\Delta\overline{\xi}$, which is equivalent to writing the relation:

$$J(\Delta\overline{\xi}) = \frac{\lambda_T}{4a}\Delta\overline{\xi} \tag{61}$$

and leads to a graphical solution of the self-consistent equations.

Depending on the context, it will be convenient to express $\Delta\overline{\xi}$ either in terms of a change $\Delta\overline{\mu}$ of the chemical potential:

$$\Delta\overline{\mu} = -\beta^{-1}\log\left(1 - \Delta\overline{\xi}\right) \tag{62}$$

or of a change of the fugacity Δz defined by:

$$\Delta\overline{z} = z\left[\mathrm{e}^{-\beta\Delta\overline{\mu}} - 1\right] = -z\Delta\overline{\xi} \tag{63}$$

but, needless to say, these three quantities remain essentially the same parameter. For an uncondensed level, (53) then provides:

$$X_{\mathbf{k}} = \frac{1}{\mathrm{e}^{\beta\widetilde{e}_k} - 1 + \Delta\overline{\xi}} = \frac{1}{1 - \Delta\overline{\xi}}\frac{1}{\mathrm{e}^{\beta(\widetilde{e}_k + \Delta\overline{\mu})} - 1}\,. \tag{64}$$

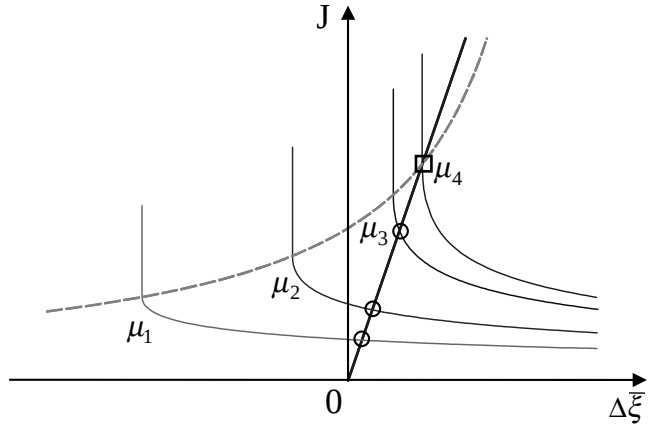

Fig. 10. Plots of the function $J(\mu, \Delta\overline{\xi})$ as a function of $\Delta\overline{\xi}$ for various values of the chemical potential μ ($\mu_1 < \mu_2 < \mu_3 < \mu_4$); for each value of the chemical potential, the solution of the coupled equations is given by the intersection point with the straight line $J = \Delta\overline{\xi}\lambda_T/4a$ (point shown with a circle in the figure). The dotted line corresponds to the hyperbolic trajectory of the singular point; the critical point ($\mu = \mu_4$) is obtained by intersecting this hyperbola with the same straight line (point shown with a square in the figure).

From (64, 60) we now get:

$$J = \frac{1}{1-\Delta\overline{\xi}} \times g_{3/2}\left[z\left(1-\Delta\overline{\xi}\right)\right] \tag{65}$$

where $g_{3/2}(z)$ is defined as usual by:

$$g_{3/2}(z) = \sum_{l=1}^{\infty} \frac{z^l}{l^{3/2}} \cdot \tag{66}$$

This function is defined only for values of z ranging from 0 to 1. Therefore, when the value of μ is fixed, the integral J is defined only for values of $\Delta\overline{\xi}$ ranging from the minimum initial value $(1 - \mathrm{e}^{-\beta\mu})$ up to one. When $\Delta\overline{\xi}$ takes this minimum value, the value of J goes to its maximum:

$$J_{\max.} = \frac{g_{3/2}(1)}{1-\Delta\overline{\xi}} = \frac{2.61..}{1-\Delta\overline{\xi}} \tag{67}$$

but, if one added the discrete contribution of the condensed ground state to the integral, the sum could take any value beyond $J_{\max.}$ for this particular value of $\Delta\overline{\xi}$, the difference being proportional to the ground state population. Figure 10 shows plots of J as a function of $\Delta\overline{\xi}$, the chemical potential μ being considered as a parameter; when μ varies, according to (67), the point of coordinates $(\Delta\overline{\xi}, J_{\max.})$ moves on a hyperbola (shown with a broken line).

For any given value of μ, equation (61) indicates that the value of $\Delta\overline{\xi}$ is obtained by intersecting the curve corresponding to J with a straight line going through the origin with slope $\lambda_T/4a$; the intersection point is shown by a circle in the figure. The construction shows that, as long as μ is very negative (classical region), $\Delta\overline{\xi}$ remains only a small correction; but the situation changes when μ approaches zero, and more and more significant corrections are introduced, provided of course the dilution parameter a/λ_T is not too small. At some critical positive value $\overline{\mu}_{\mathrm{cr.}}$, the value of $\Delta\overline{\xi}$ reaches its limit, and the system undergoes Bose-Einstein condensation[15]; this value is merely obtained by intersecting the hyperbola with the straight line, which provides:

$$\Delta\overline{\xi}_{\mathrm{cr.}} = \frac{4a}{\lambda_T}\frac{2.61..}{1-\Delta\overline{\xi}_{\mathrm{cr.}}} \simeq 2.61..\frac{4a}{\lambda_T} \cdot \tag{68}$$

Since at the transition point $\mu - \Delta\overline{\mu} = 0$, this corresponds to the following value for the chemical potential:

$$\mu = \overline{\mu}_{\mathrm{cr.}} = \Delta\overline{\mu}_{\mathrm{cr.}} \simeq \frac{10.44..}{\beta}\frac{a}{\lambda_T} \cdot \tag{69}$$

Finally, equation (56) shows that the number of particles as a function of μ is given by:

$$N = \frac{\mathcal{V}}{8\pi^3}\int \mathrm{d}^3\mathbf{k}\ \rho_{\mathbf{k}} = \frac{\mathcal{V}}{8\pi^3}\int \mathrm{d}^3\mathbf{k}\ f_1(k; \mu - \Delta\overline{\mu}). \tag{70}$$

At the critical value of the chemical potential, $\mu = \Delta\overline{\mu}$, and the degeneracy parameter $n\lambda_T^3$ is thus predicted to have exactly the same value 2.61... as for the ideal gas. Therefore, what we find within this Ursell-Dyson approximation is a relatively straightforward result: the only effect of the repulsive interactions is to change the effective value of the chemical potential, which allows positive values of μ to be reached; otherwise no change (velocity distribution, critical degeneracy parameter) is introduced.

5 Beyond mean-field: velocity dependent effects

We will now go beyond the Ursell-Dyson approximation and study which new effects are introduced by this more accurate treatment of the problem; we will see that qualitatively new effects are indeed introduced, which are strongly velocity-dependent.

5.1 A new set of equations

When (35) is added to the right hand side of (32), a new feature immediately appears: in (35), a momentum transfer $\mathbf{q}$ can now take place, introducing off-diagonal matrix

[15] The geometrical construction implies that this transition point can be reached only the value of the dilution parameter a/λ_T is sufficiently small; a simple calculation shows that this parameter should be smaller than $\left[4g_{3/2}(1)\right]^{-1}$ (which is close to 10%). If a/λ_T was larger, the trajectory of the point with coordinates $(\Delta\overline{\xi}_{\min.}, J_{\max.})$ would pass above the straight line without ever crossing it; but a/λ_T is also the parameter which determines the validity of the low energy approximation that we have made in the treatment of binary interactions, so that this situation would simply be beyond the domain of validity of the calculation.

elements[16] of U_2. In order to simplify the calculations, we will nevertheless ignore their dependence on $\mathbf{q}$ and merely assume that:

$$z^2\langle \mathbf{k},\mathbf{k}'|U_2^S|\mathbf{k}+\mathbf{q},\mathbf{k}'-\mathbf{q}\rangle = -2\frac{\lambda_T^2}{\mathcal{V}}\mathrm{e}^{-\frac{\beta}{2}\left[\widetilde{e}_{\mathbf{k}}+\widetilde{e}_{\mathbf{k}'}+\widetilde{e}_{\mathbf{k}+\mathbf{q}}+\widetilde{e}_{\mathbf{k}'-\mathbf{q}}\right]}\times a. \quad (71)$$

In Appendix C we discuss these off-diagonal matrix elements and show that this is a reasonable approximation; but it is not essential. Equation (47) is then replaced by:

$$\alpha\sum_{\mathbf{k}'}X_{\mathbf{k}'}\left[1-\frac{\alpha}{2}\sum_{\mathbf{q}}X_{\mathbf{k}+\mathbf{q}}X_{\mathbf{k}'-\mathbf{q}}\right]X_{\mathbf{k}}-\xi_k X_{\mathbf{k}}-1=0 \quad (72)$$

while the generalization to the more complete equation (37) would lead to:

$$\alpha\sum_{\mathbf{k}'}X_{\mathbf{k}'}\left[1+\frac{\alpha}{2}\sum_{\mathbf{q}}X_{\mathbf{k}+\mathbf{q}}X_{\mathbf{k}'-\mathbf{q}}\right]^{-1}X_{\mathbf{k}}-\xi_k X_{\mathbf{k}}-1=0. \quad (73)$$

We note in passing that, at each "scale of the ladder" contained in the diagrams, momentum conservation takes place, which is why the new sum extends over one index q only.

In the absence of condensation, the new term becomes an integral with a factor (density of states) proportional to the volume $\mathcal{V}$, which cancels the $\mathcal{V}^{-1}$ contained in α; the result is then independent of the volume, exactly as in the Ursell-Dyson approximation. On the other hand, it contains an extra factor a/λ_T (dilution parameter), which ensures that the additional correction is smaller than that considered in the first approximation. Now, if the ground state is condensed, X_0 becomes proportional to the volume; if $\mathbf{k}+\mathbf{k}^{'}\neq 0$, the two indices $\mathbf{k}+\mathbf{q}$ and $\mathbf{k}^{'}-\mathbf{q}$ never vanish for the same value of $\mathbf{q}$ so that X_0 now adds two constants to the integral; if $\mathbf{k}+\mathbf{k}^{'}=0$, the two indices vanish simultaneously when $\mathbf{q}=-\mathbf{k}$, so that one gets a contribution proportional to the volume. In the latter case, the sum diverges in the thermodynamic limit, a situation which never occurred in the Ursell-Dyson approximation; this is a first indication of a special coupling between opposite values of the momentum in the presence of condensation.

If only one $X_{\mathbf{k}}$ varies, while all the other are kept constant, the value of $X_{\mathbf{k}}$ is obtained as the solution of an algebraic equation; to write it explicitly, it is convenient to expand (72) term by term; when $\mathbf{k}^{'}\neq\mathbf{k}$, we obtain:

$$\alpha X_{\mathbf{k}}\sum_{\mathbf{k}'\neq\mathbf{k}}X_{\mathbf{k}'}\left[1-\alpha X_{\mathbf{k}}X_{\mathbf{k}'}-\frac{\alpha}{2}\sum_{\mathbf{q}\neq 0,\mathbf{k}\neq\mathbf{k}'}X_{\mathbf{k}+\mathbf{q}}X_{\mathbf{k}'-\mathbf{q}}\right] \quad (74)$$

[16] The matrix elements of U_2 obey a momentum selection rule, but none for energy conservation – see for instance Appendix B.

while, if $\mathbf{k}^{'}=\mathbf{k}$, the result is changed into:

$$\alpha\left(X_{\mathbf{k}}\right)^2\left[1-\frac{\alpha}{2}\left(X_{\mathbf{k}}\right)^2-\frac{\alpha}{2}\sum_{\mathbf{q}\neq 0}X_{\mathbf{k}+\mathbf{q}}X_{\mathbf{k}-\mathbf{q}}\right]. \quad (75)$$

Adding these contributions provides the equation:

$$-\frac{\alpha^2}{2}\left(X_{\mathbf{k}}\right)^4+\alpha\left(X_{\mathbf{k}}\right)^2\left[1-\frac{\alpha}{2}\sum_{\mathbf{q}\neq 0}X_{\mathbf{k}+\mathbf{q}}X_{\mathbf{k}-\mathbf{q}}-\alpha\sum_{\mathbf{k}'}\left(X_{\mathbf{k}'}\right)^2\right]-\xi_{\mathbf{k}}^{'}X_{\mathbf{k}}-1=0 \quad (76)$$

where $\xi_{\mathbf{k}}^{'}$ is now defined by:

$$\xi_{\mathbf{k}}^{\prime}=\xi_{\mathbf{k}}-\alpha\sum_{\mathbf{k}'}X_{\mathbf{k}'}+\frac{\alpha^2}{2}\sum_{\mathbf{k}'\neq\mathbf{k}}X_{\mathbf{k}'}\sum_{\mathbf{q}\neq 0,\mathbf{k}\neq\mathbf{k}'}X_{\mathbf{k}+\mathbf{q}}X_{\mathbf{k}'-\mathbf{q}}. \quad (77)$$

These results generalize (49, 50, 51); they are no longer second degree equations, since they contain higher degree terms. Nevertheless, all these terms contain one extra power of α, which is inversely proportional to the volume, so that in the thermodynamic limit they remain negligible as long as $X_{\mathbf{k}}$ is not proportional (at least) to the square root of the volume – actually, exactly as was already the case for the quadratic term in (49). Under these conditions, the situation remains essentially similar to that discussed in the preceding section, and $X_{\mathbf{k}}$ is determined by the linear terms only:

$$X_{\mathbf{k}}=-\frac{1}{\xi_{\mathbf{k}}^{'}}\cdot \quad (78)$$

The only difference is that $\xi_{\mathbf{k}}^{'}$ is now given by (77), which contains a correction proportional to α^2.

If we change sums into integrals, we get:

$$\xi_{\mathbf{k}}^{'}=\xi_{\mathbf{k}}-\Delta\overline{\xi}+\delta\xi_k \quad (79)$$

where $\Delta\overline{\xi}$ is defined as above by:

$$\Delta\overline{\xi}=4\frac{a}{\lambda_T}\left(\frac{\lambda_T}{2\pi}\right)^3\int \mathrm{d}^3\mathbf{k}' X(\mathbf{k}') \quad (80)$$

while the additional (second order) correction $\delta\xi_k$ is given by:

$$\delta\xi_k=8\left(\frac{a}{\lambda_T}\right)^2\left(\frac{\lambda_T}{2\pi}\right)^6\int \mathrm{d}^3\mathbf{k}^{'}X(\mathbf{k}^{'})\times\int \mathrm{d}^3\mathbf{q}X(\mathbf{k}+\mathbf{q})X(\mathbf{k}^{'}-\mathbf{q}). \quad (81)$$

A new feature which appears in this correction is a dependence on $\mathbf{k}$, which will introduce velocity-dependent

effects; this can be seen better by rewriting the second integral in the form:

$$\int \mathrm{d}^3\mathbf{q}' X\left(\frac{\mathbf{k}+\mathbf{k}'}{2}+\mathbf{q}'\right) X\left(\frac{\mathbf{k}+\mathbf{k}'}{2}-\mathbf{q}'\right) \qquad (82)$$

which appears as a convolution integral of the momentum distribution with itself, with a maximum when $\mathbf{k}+\mathbf{k}'=0$. As a consequence, while $X_{\mathbf{k}}$ is coupled through $\delta\xi_k$ to all other $X_{\mathbf{k}'}$'s, the maximum coupling takes place with $X_{-\mathbf{k}}$, which then implies that $\delta\xi_k$ is a larger correction near the center of the velocity distribution (because the preferred coupling occurs with $X_{\mathbf{k}'}$'s which are large) than in its wings (where velocity classes are preferentially coupled to smaller $X_{\mathbf{k}'}$'s).

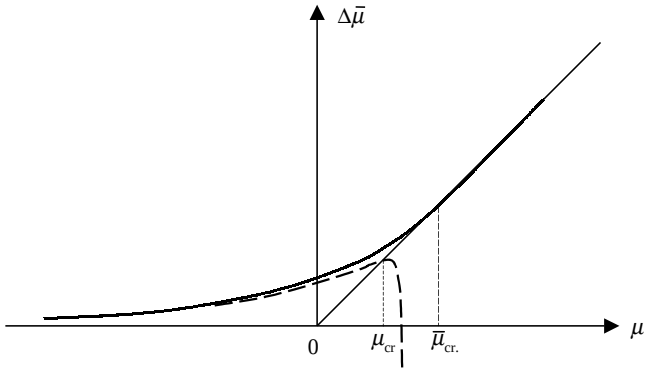

Fig. 11. Variations as a function of μ of the mean-field correction $\Delta\overline{\mu}$ to the chemical potential (full line); the corresponding critical value is $\overline{\mu}_{\mathrm{cr.}}$. A mored detailed treatment includes the extra correction $-\delta\mu_0$ (broken line) and reduces the critical value to a new value $\mu_{\mathrm{cr.}}$.

5.2 A shift in the transition parameter

As in Section 4, we have to solve equations consistently since the $X_{\mathbf{k}}$'s depend on the corrections $\Delta\overline{\xi}$ and $\delta\xi_k$ which, in turn, depend on the $X_{\mathbf{k}}$'s, a complicated problem in general. Nevertheless, we can already get a general idea of the changes introduced by the new corrections by assuming for a moment that they are known, or at least just the correction $\delta\xi_0$ for the ground state. Figure 11 then summarizes the comparison between the Ursell-Dyson approximation and the theory including $\delta\xi_0$. The full line shows the variations of $\Delta\overline{\mu}$ as a function of μ, which at $\mu=\overline{\mu}_{\mathrm{cr.}}$ reaches tangentially the straight line corresponding to the condensation condition $\mu+\Delta\overline{\mu}=0$; we note that, when $\mu\to\overline{\mu}_{\mathrm{cr.}}$ (by lower values), $\Delta\overline{\mu}$ remains a function of the chemical potential which keeps a continuous derivative[17]. The broken line illustrates the changes to this construction introduced by $\delta\xi_0$, or equivalently by the correction $\delta\mu_0$ defined by analogy with (62) (and for any value of $\mathbf{k}$) as:

$$\delta\mu_k-\Delta\overline{\mu}=\beta^{-1}\log\left(1-\Delta\overline{\xi}+\delta\xi_k\right). \qquad (83)$$

The new transition point occurs when the total effective chemical potential of the ground state vanishes:

$$\mu-\Delta\overline{\mu}+\delta\mu_0=0 \qquad (84)$$

which corresponds to a lower value $\mu_{\mathrm{cr.}}$ of the chemical potential, and no longer to a tangential contact. An interesting feature is that the square root behavior of $\Delta\overline{\mu}-\mu$ near $\mu=\overline{\mu}_{\mathrm{cr.}}$ may introduce a non-analytical behavior of the solution; in Appendix D we write down in more detail the local expansion of $\Delta\overline{\mu}$ and show, for instance, why the correction to $\mu_{\mathrm{cr.}}$ is second order in a, despite this square root behavior. Qualitatively, we can already guess that the critical value of the degeneracy parameter will be lowered in the process; this is because the excited levels get a correction $\delta\xi_k$ which is smaller than $\delta\xi_0$, and therefore experience at the new transition point an effective chemical potential which is more negative than it was in the Ursell-Dyson approach (a differential effect); but we now evaluate this correction more qualitatively.

A graphical solution of the consistent equations would be more complicated than in the preceding section, mostly because one single parameter $\Delta\overline{\xi}$ is no longer sufficient to characterize the effect of the interactions on all velocity classes. We can nevertheless resort to a "first $\delta\xi$ iteration", namely calculate the $\delta\xi_k$'s from (81) by assuming that the $X_{\mathbf{k}}$ still have the values that they had in the Ursell-Dyson approximation, and then use this correction to calculate new $X_{\mathbf{k}}$'s as well as new populations. Of course, in theory, this should be only the initial step of an iteration procedure, which should be repeated until convergence is obtained, but for the moment we limit ourselves to this first approximation.

Under these conditions, (81) becomes:

$$\delta\xi_k\simeq 4\left(\frac{a}{\lambda_T}\right)\left(\frac{\lambda_T}{2\pi}\right)^3 \mathrm{e}^{\beta\Delta\overline{\mu}} \times\int \mathrm{d}^3\mathbf{k}'\, f_1(\mathbf{k}';\mu-\Delta\overline{\mu}) J(\mathbf{k}+\mathbf{k}';\mu-\Delta\overline{\mu}) \qquad (85)$$

where the integral J is defined by:

$$J(\mathbf{K};\mu-\Delta\overline{\mu})=2\left(\frac{a}{\lambda_T}\right)\left(\frac{\lambda_T}{2\pi}\right)^3 \mathrm{e}^{2\beta\Delta\overline{\mu}} \times\int \mathrm{d}^3\mathbf{q} f_1\left(\frac{\mathbf{K}}{2}+\mathbf{q};\mu-\Delta\overline{\mu}\right) f_1\left(\frac{\mathbf{K}}{2}-\mathbf{q};\mu-\Delta\overline{\mu}\right). \qquad (86)$$

These two integrals can be calculated by expanding f_1 in series as in equation (27); integrating the Gaussian functions provides:

$$J(\mathbf{K};\mu-\Delta\overline{\mu})=2\left(\frac{a}{\lambda_T}\right)\mathrm{e}^{2\beta\Delta\overline{\mu}}\sum_{l,m}(l+n)^{-3/2} \times\exp\left\{-\frac{ln}{l+n}\frac{\lambda_T^2}{4\pi}K^2+\beta\,(l+n)\,(\mu-\Delta\overline{\mu})\right\} \qquad (87)$$

[17] Figure 10 shows that the slope of the curve giving the variations of J as a function of $\Delta\overline{\xi}$ becomes infinite when the curve connects to the vertical straight line – no discontinuity takes place in the derivative of $\Delta\overline{\xi}$ as a function of μ.

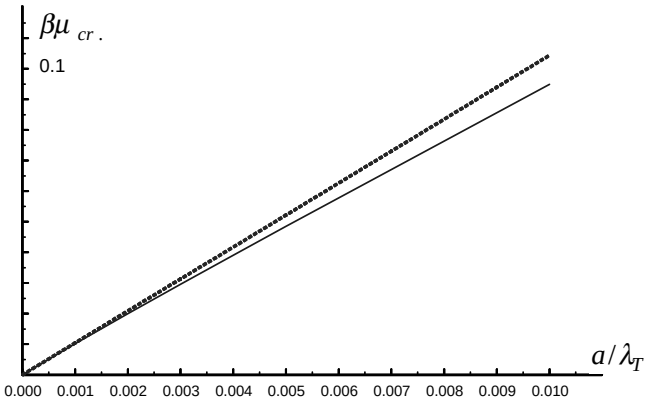

Fig. 12. Variations of the critical value of the chemical potential as a function of the dimensionless interaction parameter a/λ_T of the gas. The dotted upper straight line corresponds to the prediction of the Ursell-Dyson (mean-field) approach, equation (69); the lower line includes the velocity dependent effects, threated within the first iteration corresponding to equation (88).

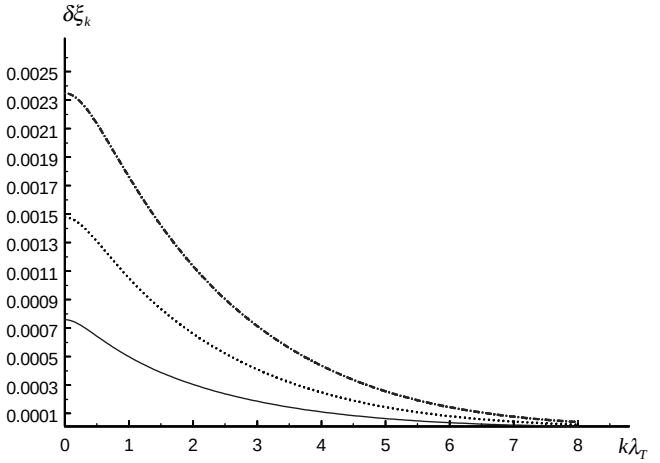

Fig. 13. Variations of the correction to the energy of the atoms as a function of their momentum, in dimensionless units $k\lambda_T$ (the half-height width of the thermal distribution is then about 4); the results are obtained by a first iteration of the non-linear equations and the value of the chemical potential is adjusted to its critical value within this approximation. The lowest curve corresponds to $a/\lambda_T = 0.002$ and its with is 1.55; the middle curve to to $a/\lambda_T = 0.003$, and its width 1.75; the upper curve is for $a/\lambda_T = 0.004$ and its width is 1.95. This shows that the velocity-dependent corrections remain localized at the center of the velocity profile.

and:

$$\delta\xi_k \simeq 8\left(\frac{a}{\lambda_T}\right)^2 \mathrm{e}^{3\beta\Delta\overline{\mu}} \sum_{l,n,p} \left[(l+n)p + ln\right]^{-3/2} \times \exp\left\{-\frac{lnp}{(l+n)\,p+ln}\,\frac{\lambda_T^2}{4\pi}k^2 + \beta\,(l+n+p)\,(\mu-\Delta\overline{\mu})\right\}. \tag{88}$$

The procedure is therefore the following: we start from an arbitrary value of μ and use the above expressions (as well as those of Sect. 4.2 for the mean-field values) to calculate the effective chemical potential (83) for each velocity class; as long as this function remains negative for all values of $\mathbf{k}$, the population $\rho_{\mathbf{k}}$ of each level is given by the direct generalization of (56):

$$\rho_{\mathbf{k}} = f_1(k; \mu - \Delta\overline{\mu} + \delta\mu_k). \tag{89}$$

Now, when μ increases, at some point condition (84) is met – see Figure 11 – and condensation takes place. Figure 12 shows a plot of the variations of this critical value of μ as a function of the dimensionless parameter a/λ_T, with, as a point of comparison, the dotted straight line obtained from the mean-field value (69); we see that the mean-field theory gives a good approximation of the value of the chemical potential.

For this critical value of μ, and for three values of the parameter a/λ_T, Figure 13 then shows the variations of $\delta\xi_k \simeq \beta\delta\mu_k$ as a function of k, in units λ_T^{-1} where the width of he thermal velocity distribution $k^2 f_1(k,0)$ is about 4. An obvious feature in the figure is that the correction $\delta\mu_k$ is neither constant (which would lead to an unchanged critical degeneracy parameter) nor a simple quadratic function of k (which would lead to an effective mass effect). In fact it has a structure within the thermal velocity distribution, which resembles a Gaussian function, and which is narrower, but not by a large factor (2 or 3 in this case); this creates a intermediate physical situation so that quantitative predictions require a somewhat more detailed study of the perturbations within the velocity profile. According to (84), the expression of the critical density can be obtained by the following summation over velocities:

$$n_{\mathrm{cr.}} = \frac{1}{(2\pi)^3}\int \mathrm{d}^3\mathbf{k}\; f_1(\mathbf{k}, \mu = \delta\mu_0 - \delta\mu_k). \tag{90}$$

This expression was used to calculate numerically the values of the critical degeneracy parameter $n\lambda_T^3$ as a function of the dilution parameter a/λ_T (also equal to $1.38..\times n^{1/3}a$ near the transition temperature); the results are shown in Figure 14, expressed in terms of the difference between this critical value and the value 2.612.. for the ideal gas. We see that the integration over velocities gives rise to a correction which turns out to be, at least approximately, linear in a/λ_T. As a point of comparison, we also show (lowest line) the results of a recent path integral quantum Monte-Carlo calculation [32]; the agreement is satisfactory but not perfect; below we discuss possible improvements.

At this point, it becomes possible to discuss in more detail the physical origin of these results. Mathematically, the key role in the mechanism is played by $\delta\xi_{\mathbf{k}}$, a correction which tends to increase effective chemical potential of a velocity class $\mathbf{k}$, while $\Delta\xi$ had just the opposite effect. In other words, the mean-field approximation tends to overestimate the repulsion between the velocity classes, so that a correction with the opposite sign is introduced by $\delta\xi_{\mathbf{k}}$; the correction is more important for low velocity classes than for rapid particles. Physically, it is indeed natural

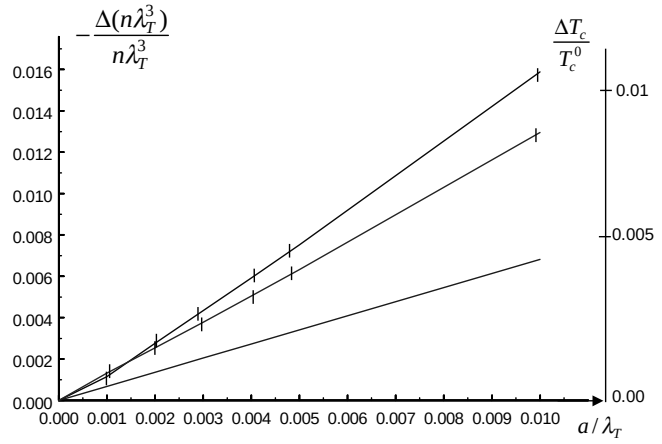

Fig. 14. Relative changes of the degeneracy parameter $n\lambda_T^3$ as a function of the ratio a/λ; the left vertical axis gives the opposite of this (negative) change, while the right vertical axis corresponds to the equivalent (positive) change of the critical temperature at constant density. The lower line shows the results of the quantum Monte-Carlo calculations of reference [32]; the upper curve corresponds to the results of our calculation within the first iteration of Section 5.2; the middle curve to the more elaborate calculation discussed at the end of Section 5.3, where a denominator $1+J(\mathbf{k}+\mathbf{k}')$ is added within the integral giving $\delta\xi_k$ (but still with only one iteration of the non linear equations).

to expect that slow particles should be more sensitive to interactions than fast particles: they can more easily rearrange themselves spatially in order to minimize their repulsive interactions. By contrast, fast particles have too much kinetic energy to have the same sensitivity to small perturbations; the rearrangement does not take place, so that they experience the full mean repulsion $\Delta\overline{\xi}$ (as for uncorrelated particles). The velocity dependence of the correction shown in Figure 13; at the critical temperature, the populations of the low $\mathbf{k}$ levels are almost those of the ideal gas, with only a mass renormalization effect introduced by the curvature of the curve at the origin; but those of higher velocities levels get almost no correction $\delta\xi_{\mathbf{k}}$, so that they remain smaller than those of the ideal gas with chemical potential $\mu-\Delta\overline{\mu}$. Since the calculation of the change of the degeneracy parameter $n\lambda_T^3$ requires an integration over all velocities – not only low velocities – we see that the effect can not be understood within an effective mass description only; indeed, a more precise description of the change of the spectrum at all values of k is necessary.

Our results go in the same direction than the views expressed by Nozières [19] concerning the effects of repulsive interactions in a Bose gas, which were found to stabilize the gas against smeared condensation (fractionned condensate): Figure 12 predicts that the populations of the low excited levels are indeed lower than they would be in an ideal gas (assuming a bare mass for the particles), which is an indication or a stronger tendency to populate the ground state exclusively. The physical origin of the effect is nevertheless rather different: reference [19] is based on the use of a mean-field calculation, where no rearrangement (or change of the velocity profile) can take place; here we find that the changes originate from a differential effect which is essentially beyond mean-field theory. Also, [19] treats a system which is already condensed, while we approach the transition from the non-condensed phase, so that the physics may well be different in both cases. We finally note that the effective mass effect at the center of Figure 11 is of different nature than that calculated in [28]; in particular, it does not require the potential to have a finite range to occur (also, it has the opposite sign: we find a smaller effective mass than the bare mass).

5.3 Discussion; a change in the dispersion relation

The calculations that we have developed are not exact, for two reasons:

(i) we have not solved the coupled equations between the $\delta\xi_{\mathbf{k}}$'s and the $X_{\mathbf{k}}$, but only a "first $\delta\xi$ iteration" of these equations;

(ii) the initial equation (72) is not exact; (73) is a better approximation, but not exact either, and can be completed with a larger class of diagrams.

When approximation (i) is not made, equations (85–90) are replaced by a system containing, first, the equations providing the $X_{\mathbf{k}}$'s:

$$X_{\mathbf{k}}=\frac{f_1\left[\mathbf{k},z(1-\Delta\overline{\xi}+\delta\xi_{\mathbf{k}})\right]}{1-\Delta\overline{\xi}+\delta\xi_{\mathbf{k}}} \tag{91}$$

and, second, the equations providing the $\delta\xi_{\mathbf{k}}$'s (the mean repulsion $\Delta\overline{\xi}$ keeps the same expression as in the mean-field theory):

$$\delta\xi_{\mathbf{k}}=4\left(\frac{a}{\lambda_T}\right)\left(\frac{\lambda_T}{2\pi}\right)^3\int \mathrm{d}^3\mathbf{k}' X_{\mathbf{k}'}\times J(\mathbf{k}+\mathbf{k}') \tag{92}$$

with:

$$J(\mathbf{K})=2\left(\frac{a}{\lambda_T}\right)\left(\frac{\lambda_T}{2\pi}\right)^3\int \mathrm{d}^3\mathbf{q}\, X_{\mathbf{q}+\mathbf{K}/2}\times X_{-\mathbf{q}+\mathbf{K}/2}. \tag{93}$$

We do not intend to solve these coupled equations in detail here, but just to discuss in general terms what kind of new physical effects they introduce, as compared to those of the preceding section. A first indication can be obtained by studying what would have been obtained in a "second $\delta\xi$ iteration". Instead of the expressions (85, 86) containing ordinary Bose-Einstein distributions, we would have inside the integrals perturbed distributions, with already a relatively narrow enhancement near the center due to the first iteration. The narrowing effect of the auto-convolution integral, which occurred in the first step, would take place again, so that we would get a still more localized perturbation at the center of the velocity profile. Now, when more and more iterations are added, narrower and narrower perturbations are expected to be introduced at the center, so that at the end there

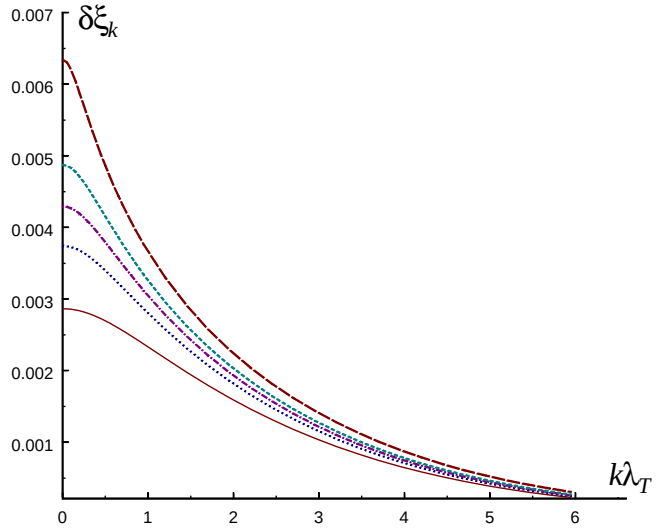

Fig. 15. When more and more iterations are performed in the calculation of the corrections to the energy of the particles, a sharper and sharper localized perturbation occurs at low velocities, so that eventually the spectrum no longer remains quadratic at the origin, but acquires a dependence in $k^{-3/2}$.

is no reason why the correction to the energy should remain quadratic at the origin. The situation is shown in Figure 15.

Actually, this can also be seen from the fact that (92) gives a divergent integral[18] at the critical value of the chemical potential if the $X_{\mathbf{k}}$'s diverge at the origin as k^{-2}; such a divergence would be incompatible with the relation $\mu - \Delta\overline{\mu} + \delta\xi_0 = 0$ at the transition point, as visible for instance in Figure 11. In other words, the integral giving $\delta\xi_0$ plays the role of a restoring force in the problem, and the solution has to adapt to keep it finite. Assume then that, at the condensation point, the variations $\delta\xi_k$ for small values of k correspond to a spectrum with a power α of the momentum:

$$\delta\xi_0 - \delta\xi_k \simeq k^{\alpha}. \tag{94}$$

Then, for small velocities, the populations are proportional to:

$$X_k \simeq k^{-\alpha}. \tag{95}$$

Now insert these expression into expressions (92, 93); since $\delta\xi_k$ is given by a 6 dimension integral of three quantities which vary as $k^{-\alpha}$, we get the relation:

$$k^{6-3\alpha} = k^{\alpha} \tag{96}$$

or:

$$\alpha = \frac{3}{2}\cdot \tag{97}$$

[18] The first iteration (85) of (92) already diverges, as the logarithm of $|\mu - \Delta\overline{\mu}|$ [46]; this divergence is taken into account in Figure 10.

In the above reasoning, we have implicitly assumed that the behavior of $\delta\xi_k$ for small values of k depends only on the domain of integration close to the origin; our result is then consistent since a function in $k^{3/2}$ will dominate over a quadratic function as long as k is sufficiently small. We recover in this way the modified spectrum already obtained in a different context by Patashinskii and Pokrovskii [47].

As far as the second approximation is concerned, the simplest possibility to go beyond it is to include more diagrams and to use (73) instead of (72), which amounts to adding a denominator $1 + J(\mathbf{k} + \mathbf{k}')$ under $J(\mathbf{k} + \mathbf{k}')$ inside the integral (92). The analytical algebra then becomes even more complicated, but we have performed some of the corresponding numerical calculations. The results are shown in the middle line in Figure 14: indeed, they are in better agreement with the quantum Monte-Carlo results than the more crude approximation made before. One could therefore hope that a really good agreement would be attainable by including a larger class of diagrams in our calculations. It is also interesting to note that our conclusion concerning the exponent $\alpha = 3/2$ remains valid in this case, as actually also when a broader class of diagrams is added in the integral equation for ρ_1; this is because more and more diagrams can be generated in a process where one U_2 is added, bringing with it two X's, but also one momentum integration, a process in which the low k dependence of $\delta\xi_0 - \delta\xi_k$ is multiplied by $k^{3-2\alpha}$, a constant if $\alpha = 3/2$. Nevertheless, the exponent is not that expected from the universality class of the transition, which would be closer to the value $\alpha = 2$; this might indicate that, very close to the transition point, logarithmic terms that we have not included in our evaluation of the power counting become important.

6 Conclusion

Our study show that the effect of repulsive interactions is to shift the degeneracy parameter by an amount:

$$\frac{\Delta(n\lambda_T)_{\text{cr.}}}{(n\lambda_T)_{\text{cr.}}} \simeq -1.3\frac{a}{\lambda_T} \simeq -(na^3)^{1/3} \tag{98}$$

or, in terms of a shift of critical temperature of the gas at constant density:

$$\frac{\Delta T_{\text{c}}}{T_{\text{c}}} \simeq \frac{a}{\lambda_T} \simeq 0.7(na^3)^{1/3} \tag{99}$$

where a is the scattering length (assumed to be positive) of the interaction potential and λ_T the thermal wavelength of the atoms. In the case of hard cores, these results are about 80% larger than those resulting from the numerical calculations of [32], which provides a reasonable agreement in view of the approximations that we have made when solving the final non-linear equations; in fact, it is possible that more extensive calculations would lead to a closer agreement. A striking feature of the results of [32] is the presence of two regimes, due to the increase of T_{c} at low

densities introduced by the repulsive interactions, followed by a decrease at higher densities. This is not an obvious phenomenon: usually interactions tend to mask quantum effects and not to enhance them, so that one could naturally expect a constant decrease of the transition temperature as a function of density. Our approach explains this feature naturally, in terms of a microscopic re-arrangement mechanism which, in essence, automatically leads to an increase of this temperature (for repulsive interactions); the re-arrangement produces an enhancement of the velocity distribution at its center, which develops just above the transition temperature as a precursor, and allow the gas to reach the transition point before its density (integrated over all velocities) reaches the critical density of the ideal gas. In this picture, the mechanism for superfluidity is inherently different from Bose-Einstein condensation in an ideal gas: in a sense one could say that superfluidity triggers condensation, and that this phenomenon takes place at a lower density (or higher temperature) than in a mean field picture. At the transition point, the distortion of the velocity distribution bears some similarity with the results of a Bogolubov transformation (where significant changes of the populations are also introduced for low energy levels); the corresponding spectrum is not linear, but contains an exponent 3/2, which can be seen as an intermediate value between the high temperature and low temperature regimes, as already pointed out in [47]. In a future article, we intend to extend our theory to lower temperatures and condensed gases in order to make a more precise contact with this transformation. One can also remark that the singular behavior of the mean-field theory near the transition point introduces non-analyticities in the results, mixing up together various orders in the natural expansion parameter a/λ_T; the presence of a square root in the calculations makes it necessary to push the calculation to higher orders than one would naively expect. This suggest that theories using pseudopotentials may quickly reach their limit, since they are based on expressions of the matrix elements which are valid up to the second power of the potential range; from third order, the behavior of wave functions inside the interaction potential (particles in the middle of a collision) becomes relevant, so that an Ursell approach would be safer.

Concerning the high density regime, it remains for the moment beyond the domain of validity of our calculations: in denser systems, a treatment in terms of Ursell operators or rank exceeding 2 would become necessary. Doing so, one could then hope to see how a mean attractive field develops in order to stabilize a liquid, even before Bose-Einstein condensation is reached – in other words, develop a more complete theory predicting the existence of two transitions (ordinary liquefaction and superfluid transition, as in helium four). But denser systems do not only differ from gases because of the presence of an attractive mean field; the atomic motions are also hindered by the interactions for lack of space, so that the spatial rearrangement which can easily take place in a gas is no longer possible. The physics of the effects of the interactions on exchange and on the critical temperature of Bose-Einstein transition is therefore significantly different. In a similar perspective, we note that several of the integrals that have been introduced in the treatment beyond the Ursell-Dyson approximation are mathematically different from those of a mean-field treatment: higher dimensions integrals, etc. In other words, the dimensional properties of the transition may be significantly altered by the interactions; this is another possibility that should be explored.

Another approximation which could be released is ignoring the changes as a function of the relative momentum of the Ursell length (or the scattering length), which we have treated as exactly constant; moreover, we have not included the energy dependence of the off-diagonal matrix elements of U_2. A better treatment could for instance include a quadratic dependence on the relative momentum; one could then reasonably expect to recover the effective mass effect predicted in [28], since it is precisely due to a k dependence of the matrix elements; in other words one should get a better approximation to the full density variations predicted in [32], hopefully including a maximum in the critical temperature. Finally, it could also be interesting to explore the effects of resonant changes of the cross sections at very low energies on the transition temperature, since they seem to be now accessible [48–50]. One could imagine situations where sharp variations of the cross section could completely change the character of the Bose-Einstein transition, maybe even to a point where condensation would not involve a single level but, for instance, all levels on the surface of a sphere corresponding to a given length of k; this would be another kind of realization of the smeared condensation mentioned in the introduction.

The preliminary stages of this work were initiated during visits to the Kamerlingh Onnes Laboratorium in Leiden and the Blackett Laboratory at Imperial College (London). The hospitality of Profs. G. Frossati, J.P. Connerade, H. Hutchinson and N. Rivier played an essential role in making these visits fruitful. Discussions with Philippe Nozières, Sandro Stringari, Alex Meyerovich, Antony Leggett and Edouard Brézin were especially useful. The final part of this work was made during a very stimulating visit at the Institute of Theoretical Physics at the University of California at Santa Barbara.

This research was supported in part by the National Foundation under Grant No. PHY94-07194.

Note added in proof

It has been pointed out to us by G. Baym that our results can also be obtained in the language of Green functions and self energies; this generalization will be the object of a future publication in collaboration [51].

Appendix A: Expansion of the solution of an integral equation

In this appendix, we study the solution of equation obtained by adding (36) to the right hand side of (33):

$$\rho_1(1) = f_1(1) + 2xz^2\,[1+f_1(1)] \times \mathrm{Tr}_2\left\{W(1,2) + [W(1,2)]^2\right\} \quad \text{(A.1)}$$

(for convenience, a variable x has been introduced in front of the trace but, at the end of the calculation, we can set $x=1$) where:

$$W(1,2) = U_2^S(1,2)\,[1+\rho_1(1)]\,[1+\rho_1(2)]\,. \quad \text{(A.2)}$$

We show, by a series expansion in powers of x, that this integral equation gives correct weights (in fact, weights equal to one) to all diagrams that it introduces; a similar proof could be made for the more general equation (37). If we expand the solution of (A.1) in powers of x:

$$\rho_1(1) = \sum_{n=0}^{\infty} x^n \rho_1^{(n)}(1) \quad \text{(A.3)}$$

we get from (A.1) the following recurrence relation:

$$\rho_1^{(n)}(1) = 2z^2\,[1+f_1(1)]\,\mathrm{Tr}_2\Bigg\{U_2^S(1,2) \times \sum_{q=0}\left[\delta_{q,0}+\rho_1^{(q)}(1)\right]\left[\delta_{n-q,0}+\rho_1^{(n-q-1)}(2)\right] + U_2^S(1,2) \times \sum_{q+q'+q''+q'''=n-1}\left[\delta_{q,0}+\rho_1^{(q)}(1)\right]\left[\delta_{q',0}+\rho_1^{(q')}(2)\right] \times U_2^S(1,2)\left[\delta_{q'',0}+\rho_1^{(q'')}(1)\right]\left[\delta_{q''',0}+\rho_1^{(q''')}(2)\right]\Bigg\} \quad \text{(A.4)}$$

for $n \neq 0$; for $n=0$ we get:

$$\rho_1^{(0)}(1) = f_1(1). \quad \text{(A.5)}$$

Although equation (A.4) looks complicated, its content is actually simple; it describes how the structure of the diagrams contained in $\rho_1^{(n)}(1)$ is built from the "root" of the diagram, progressing along the lowest horizontal cycle/line, and adding branches made of lower orders. For example, let us first discuss direct terms, those for which U_2^S can be merely replaced by U_2. When the first U_2 operator occurs along the lowest horizontal line, two cases are possible: either this operator introduces a new horizontal line (cycle) which is not connected anymore to the root line by any other U_2, and this case corresponds to the first line in the right hand side of (A.4)); or it introduces a new horizontal line which is connected again by another U_2 to the root line, corresponding to the second and third line in (A.4). In the first case, two sub-diagrams are branched after this first U_2, as shown by the arrows in the fist diagram of Figure 16; they can occur in n possible ways (this corresponds to the summation over q), combining all possible lower orders to get a sum of orders equal to $n-1$; first, the lower connection is replaced by a dotted line symbolizing $1+f_1(1)$ (the sum of $U_1(1)$ to all powers ranging from 1 to infinity) while the upper line contains the diagrams contained in $\rho_1^{(n-1)}$; second, the lower connection gets $\rho_1^{(1)}$ while the upper connection gets $\rho_1^{(n-2)}$, etc. In the second case, the basic idea is the same, except that now the lower orders $\rho_1^{(q)}$ are plugged in at four different places, as symbolized in the second diagram of Figure 16.

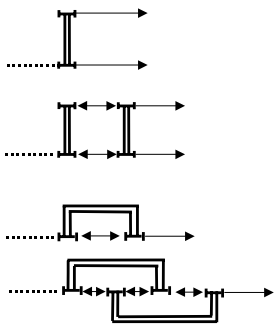

Fig. 16. Diagrams summarizing the construction of $\rho_1^{(n)}$ as a function of $\rho_1^{(n-1)}$.

As for the exchange terms, where U_2^S is replaced by $U_2^S P_{\mathrm{ex.}}$, they are very similar, except that the first U_2 reconnects to the root cycle, as shown in the third and fourth diagrams in Figure 16. Finally, direct and exchange connections can be combined in any way so that, eventually, all diagrams corresponding to the class considered are generated. By recurrence we see that, if any direct Ursell diagram was contained once and only once in $\rho_1^{(n-1)}$, it will also be contained once and once only at order n in $\rho_1^{(n)}$. The integral equation therefore ascribes weights to all diagrams which are 1, as expected. It therefore gives an appropriate description of the approximation considered, where two cycles are never connected more than twice.

The generalization to any number of connections is the purpose of equation (37); it can bee checked in the same way that it corresponds to appropriate weights for all the diagrams.

Appendix B: A potential minimization solution of the non linear equations

Define the potential:

$$\Phi = \frac{1}{2}\sum_{\mathbf{k},\mathbf{k}'}\alpha_{\mathbf{k},\mathbf{k}'}X_{\mathbf{k}}X_{\mathbf{k}'} - \sum_{\mathbf{k}}\left(\xi_{\mathbf{k}}X_{\mathbf{k}} + \log X_{\mathbf{k}}\right). \quad \text{(B.1)}$$

It is stationary under the conditions:

$$\frac{\partial\Phi}{\partial X_{\mathbf{k}}} = \sum_{\mathbf{k}'}\alpha_{\mathbf{k},\mathbf{k}'}X_{\mathbf{k}'} - \xi_{\mathbf{k}} - \frac{1}{X_{\mathbf{k}}} = 0, \quad \text{(B.2)}$$

which, assuming $X_{\mathbf{k}} \neq 0$, is equivalent to (47) (actually to a more general version of these equations where all $\alpha_{\mathbf{k},\mathbf{k}'}$ are not necessarily equal). The solution of the non-linear equations of the Ursell-Dyson approximation can therefore be obtained by a potential minimization of the function Φ.

Assume for instance that all $X_{\mathbf{k}}$'s except two, X_0 and X_1, are kept constant. We set:

$$\begin{array}{l} S = X_0 + X_1 \\ D = X_0 - X_1 \end{array} \tag{B.3}$$

and:

$$\begin{array}{l} \xi_0^{'} = \xi + \lambda \\ \xi_1^{'} = \xi + \lambda \end{array} \tag{B.4}$$

so that the potential function becomes, within terms which do not depend on X_0 and X_1(from now on we assume that all α's are equal):

$$\Phi = \frac{\alpha}{2} S^2 - \xi S - \lambda D - \log\left[S^2 - D^2\right] + ... \tag{B.5}$$

We now write:

$$\begin{array}{l} \dfrac{\partial \Phi}{\partial S} = \alpha S - \xi - \dfrac{2S}{S^2 - D^2} \\ \dfrac{\partial \Phi}{\partial D} = -\lambda + \dfrac{2S}{S^2 - D^2}. \end{array} \tag{B.6}$$

The second equation provides a quadratic equation in D with the solution:

$$D = \frac{1}{\lambda}\left[-1 \pm \sqrt{1 + \lambda^2 S^2}\right] \tag{B.7}$$

but it is easy to see that only the root with the + sign in front of the radical is acceptable: in (45), the $X_{\mathbf{k}}$'s are defined as positive quantities, and the other solution would lead to $D < S$. For a system contained in a box of size L, the energy difference between the ground state and the first excited level is proportional to L^{-2}, so that the same is true for λ; now, if we assume that the sum of the populations S is macroscopic, we have $S \sim L^3$ and $\lambda S \gg 1$. Then:

$$D \simeq \frac{1}{\lambda}\left[\lambda S\left(1 + \frac{1}{2(\lambda S)^2}\right) - 1\right] = S - \frac{1}{\lambda} \tag{B.8}$$

which is, as S, proportional to L^3. We see that:

$$\begin{array}{l} X_1 = (S - D)/2 \sim L^2 \\ X_0 = (S + D)/2 \sim L^3 \end{array} \tag{B.9}$$

which is similar to the situation for the ideal gas. Finally, S is given by the first equation (B.6):

$$\frac{\partial \Phi}{\partial S} = 0 = \alpha S - \xi - \frac{2S}{2D/\lambda} = \alpha S - \xi - \lambda \tag{B.10}$$

which provides:

$$S \simeq \frac{\xi_1^{'}}{\alpha} \sim \mathcal{V}. \tag{B.11}$$

The advantage of the potential method is that it allows one to go beyond the continuous (integral) approximation of $\Delta\overline{\xi}$ and to study what happens to each discrete level; it would be interesting to generalize the method to equations (72, 73) in order to check the quality of the conjectures made in Section 5.3 concerning the linear character of the velocity profile near the center.

Appendix C: Matrix elements of U_2

In this appendix we give a perturbative calculation of the matrix elements of U_2; for a strong potential of range b, replacing the real potential by a pseudopotential [25,26], the calculation remains valid up to second order in b. The first order value of the part of U_2 which acts in the space of relative motion of the two particles is:

$$U_2^{\text{rel.}} = -\int_0^{\beta} \mathrm{d}\beta' \, \mathrm{e}^{-(\beta-\beta')H_0} V_2 \mathrm{e}^{-\beta' H_0} + ... \tag{C.1}$$

where H_0 is the kinetic energy Hamiltonian. From this we get, still in the space or the relative motion:

$$\langle \varkappa | U_2^{\text{rel.}} | \varkappa' \rangle = \overline{V}_2(\varkappa' - \varkappa) \frac{\mathrm{e}^{-\beta\epsilon(\varkappa')} - \mathrm{e}^{-\beta\epsilon(\varkappa)}}{\epsilon(\varkappa') - \epsilon(\varkappa)} + ... \tag{C.2}$$

where:

$$\epsilon(\varkappa) = \frac{\hbar^2 \varkappa^2}{m} \tag{C.3}$$

is the kinetic energy and $\overline{V}_2(\mathbf{k})$ the Fourier transform of the interaction potential $V_2(\mathbf{r})$. Coming back to the full space of two interacting particles, we set:

$$\begin{array}{l} \mathbf{k}_1 = \dfrac{\mathbf{K}}{2} + \varkappa \; \mathbf{k}_1' = \dfrac{\mathbf{K}}{2} + \varkappa' \\ \mathbf{k}_2 = \dfrac{\mathbf{K}}{2} - \varkappa \; \mathbf{k}_2' = \dfrac{\mathbf{K}}{2} - \varkappa' \end{array} \tag{C.4}$$

(if $\varkappa \neq \varkappa'$, the kinetic energy is not conserved for the relative motion, while it is always for the center of mass motion; in the same way, the total momentum is always conserved). We the have:

$$\langle \mathbf{k}_1, \mathbf{k}_2 | U_2(1,2) | \mathbf{k}_1', \mathbf{k}_2' \rangle = \mathrm{e}^{-\beta E_K} \overline{V}_2(\mathbf{q}) \frac{\mathrm{e}^{-\beta\epsilon(\varkappa')} - \mathrm{e}^{-\beta\epsilon(\varkappa)}}{\epsilon(\varkappa') - \epsilon(\varkappa)} + ... \tag{C.5}$$

where E_{K} is the kinetic energy of the center of mass:

$$E_{\mathrm{K}} = \frac{\hbar^2 K^2}{4m} \tag{C.6}$$

and $\mathbf{q}$ is the transferred momentum:

$$\mathbf{q} = \varkappa - \varkappa'. \tag{C.7}$$

With this result, if we set:

$$z^2\langle \mathbf{k},\mathbf{k}^{'}|U_2^S|\mathbf{k}+\mathbf{q},\mathbf{k}^{'}-\mathbf{q}\rangle = -4\frac{\lambda_T^2}{\mathcal{V}}\mathrm{e}^{-\frac{\beta}{2}\left[\widetilde{e}_{\mathbf{k}}+\widetilde{e}_{\mathbf{k}'}+\widetilde{e}_{\mathbf{k}+\mathbf{q}}+\widetilde{e}_{\mathbf{k}'-\mathbf{q}}\right]}\times a(\mathrm{non-diagonal}) \tag{C.8}$$

we get:

$$a(\mathrm{non-diagonal}) = \overline{V}_2(\mathbf{q})\frac{\sinh\beta\left[\widetilde{e}(\varkappa^{'})-\widetilde{e}(\varkappa)\right]}{\beta\left[\widetilde{e}(\varkappa^{'})-\widetilde{e}(\varkappa)\right]} \tag{C.9}$$

which shows that the off diagonal matrix elements remain comparable to the diagonal elements within the thermal profile, with a factor of approximately 2.

Appendix D: Calculating the correction to the chemical potential introduced by velocity-dependent effects

Equations (61, 65), together with the definition (62) of $\Delta\overline{\mu}$, provide the relation:

$$\Delta\overline{\xi} = \frac{4a}{\lambda_T}\frac{1}{1-\Delta\overline{\xi}}g_{3/2}\left[z\left(1-\Delta\overline{\xi}\right)\right] \tag{D.1}$$

which can also be written as:

$$\mathrm{e}^{-\beta\Delta\overline{\mu}}-\mathrm{e}^{-2\beta\Delta\overline{\mu}} = \frac{4a}{\lambda_T}g_{3/2}\left[\mathrm{e}^{\beta(\mu-\Delta\overline{\mu})}\right]. \tag{D.2}$$

Writing the same relation for the particular value of μ:

$$\mu = \overline{\mu}_{\mathrm{cr.}} = \Delta\overline{\mu}_{\mathrm{cr.}} \tag{D.3}$$

provides:

$$\mathrm{e}^{-\beta\Delta\overline{\mu}_c}-\mathrm{e}^{-2\beta\Delta\overline{\mu}_c} = \frac{4a}{\lambda_T}g_{\max.} \tag{D.4}$$

where:

$$g_{\max.} = g_{3/2}(1) = 2.612... \tag{D.5}$$

Now, by difference, we obtain:

$$\begin{aligned}\mathrm{e}^{-\beta\Delta\overline{\mu}}-\mathrm{e}^{-\beta\Delta\overline{\mu}_c}-\mathrm{e}^{-2\beta\Delta\overline{\mu}}+\mathrm{e}^{-2\beta\Delta\overline{\mu}_c} &= \frac{4a}{\lambda_T}\left[g_{3/2}\left[\mathrm{e}^{\beta(\mu-\Delta\overline{\mu})}\right]-g_{\max.}\right]\\ &\simeq -\frac{4a}{\lambda_T}c\sqrt{\beta\left(\mu\right)-\Delta\overline{\mu}}\end{aligned} \tag{D.6}$$

where the numerical coefficient c is given by (see [44] or exercise 12.3 of [25]):

$$c = 3.544.. \tag{D.7}$$

From this we obtain:

$$\beta\left(\mu-\Delta\overline{\mu}\right) = \left(\frac{\lambda_T}{4a}\right)^2 c^{-2}\left[\mathrm{e}^{-\beta\Delta\overline{\mu}}-\mathrm{e}^{-\beta\Delta\overline{\mu}_c}-\mathrm{e}^{-2\beta\Delta\overline{\mu}}+\mathrm{e}^{-2\beta\Delta\overline{\mu}_c}\right]^2 \tag{D.8}$$

or:

$$\beta\left(\mu-\Delta\overline{\mu}\right) = \left(\frac{\lambda_T}{4a}\right)^2 c^{-2}\left[\beta\left(\Delta\overline{\mu}-\Delta\overline{\mu}_c\right)\right]^2+... \tag{D.9}$$

But, to this order, we can replace $\Delta\overline{\mu}$ by μ in the right hand side:

$$\beta\left(\mu-\Delta\overline{\mu}\right) = \left(\frac{\lambda_T}{4a}\right)^2 c^{-2}\left[\beta\left(\mu-\Delta\overline{\mu}_c\right)\right]^2+... \tag{D.10}$$

At the critical point, $\mu+\delta\mu_0-\Delta\overline{\mu}=0$ so that this relation becomes:

$$\beta\delta\mu_0 \simeq \left(\frac{\lambda_T}{4a}\right)^2 c^{-2}\left[\beta\left(\mu-\Delta\overline{\mu}_c\right)\right]^2+... \tag{D.11}$$

or:

$$\beta\left(\overline{\mu}_{\mathrm{c}}-\mu_{\mathrm{c}}\right) \simeq \frac{4a}{\lambda_T}c\sqrt{\beta\delta\mu_0} \tag{D.12}$$

which is second order in a/λ_T (since $\delta\mu_0$ is second order in this quantity).

References

1. A. Einstein, Preussische Akademie der Wissenschaften, Phys. Math. Klasse, Sitzungsberichte, 3 (1925).
2. W.A. Blanpied, Am. J. Phys. **40**, 1212 (1972).
3. O. Theimer, Budth Ram, Am. J. Phys. **45**, 242 (1977).
4. W.E. Lamb, Phys. Rev. **59**, 677 (1941).
5. A. Pais, *The Science and Life of Albert Einstein* (Oxford University Press, 1982), Chapter 23; see in particular section 23d. (3).
6. Albert Einstein, *Oeuvres Choisies*, Vol. 1 Quanta (Seuil CNRS Paris, 1989), Chapter 12.
7. G.E. Uhlenbeck, *Some reminiscences about Einstein's visit to Leiden*, epilogue in Proceedings Einstein Centennial Symposium 1979 *Some strangeness in the proportion* (H. Woolf dir.) (Reading (Mass.), Addislon Wesley, 1980).
8. R. Balian, *From microphysics to macrophysics* (Springer Verlag, 1992), Vol. II, Section 12.3.1.
9. T.J. Greytak, D. Kleppner, *Lectures on spin polarized hydrogen*, in *Tendances actuelles en physique atomique*, edited by G. Gryndberg, R. Stora (Elsevier, 1984).
10. R. Balian, Loc. Cit., exercises 12.b and 12.c.
11. H.D. Politzer, Phys. Rev. A **54**, 5048 (1996).
12. F. London, Nat. **141**, 643 (1938); Phys. Rev. **54**, 947 (1938).
13. O. Penrose, L. Onsager, Phys. Rev. **104**, 576 (1956).
14. S.T. Beliaev, J. Ekptl. Theoret. Phys. **34**, 417 (1958); Soviet Physics JETP **34**, 289 (1958).
15. C.N. Yang, Rev. Mod. Phys. **34**, 694 (1962).
16. J. Gavoret, P. Nozières, Ann. Phys. **28**, 349 (1964).

17. H. Fröhlich, Phys. Kond. Materie **9**, 350 (1969) and references contained.
18. M. Girardeau, *Phys. Fluids* **5**, 1468 (1962); see also J. Math. Phys. **11**, 684 (1970), especially Section 9.
19. P. Nozières, in *Bose-Einstein condentation*, edited by A. Griffin, D.W. Snoke, S. Stringazri (Cambridge University Press, 1995).
20. M. Luban, Phys. Rev. **128**, 965 (1962); see in particular Chapter I: "To our knowledge there exists no treatment which obtains (the Einstein condensation) as a derived result, in contrast to an assumption made at the outset, in a nonideal boson gas. Instead, one obtains a posteriori inference that such is fact".
21. van der Berg, J.T. Levis, P. de Smedt, J. Stat. Phys. **37**, 697 (1984).
22. D.M. Ceperley, Rev. Mod. Phys. **67**, 279 (1995).
23. P.E. Sokol, in *Bose-Einstein condensation*, edited by A. Griffin, D.W. Snoke, S. Stringari (Cambridge University Press, 1995).
24. V.V. Goldman, I.F. Silvera, A.J. Leggett, Phys. Rev. B **24**, 2870 (1981).
25. K. Huang, *Statistical Mechanics* (Wiley, 1963), Section 13.3; 2nd edn. (1987), Section 10.5.
26. K. Huang, C.N. Yang, Phys. Rev. **105**, 767 (1957); K. Huang, C.N. Yang, J.M. Luttinger, Phys. Rev. **105**, 776 (1956); T.D. Lee, K. Huang, C.N. Yang, Phys. Rev. **106**, 1135 (1957).
27. K. Huang, *Imperfect Bose gas*, in Studies in Statistical Mechanics Vol. II, edited by J. de Boer, G.E. Uhlenbeck (North Holland, 1964); see in particular Chapter 5 (where Fig. 5.5 is incorrectly drawn since it shows a reduced critical temperature).
28. A. Fetter, J.D. Walecka, *Quantum theory of many-particle systems* (Mc Graw Hill, 1971), see Chapter 28.
29. T. Toyoda, Ann. Phys. (N.Y.) **141**, 154 (1982).
30. H.T.C. Stoof, Phys. Rev. A **45**, 8398 (1992).
31. M. Bijlsma, H.T.C. Stoof, Phys. Rev. A **54**, 5085 (1996).
32. P. Grüter, D. Ceperley, F. Laloë, Phys. Rev. Lett. **79**, 3549 (1997).
33. M. Holzmann, W. Krauth, M. Narachewskii, Phys. Rev. A **59**, 2956 (1999).
34. E.M. Lifshitz, L.P. Pitaevskii, Landau, Lifshitz, *Course of Theor. Phys.* Vol. 9, Statistical Physics (Pergamon Press, 1980), Chapter III.
35. E.P. Gross, Journ. Math. Phys. **4**, 195 (1963).
36. F. Dafolvo, S. Giorgini, L. Pitaevskii, S. Stringari, Rev. Mod. Phys. **71**, 463 (1999).
37. P. Grüter, F. Laloë, J. Phys. I France **5**, 181 (1995).
38. P. Grüter, F. Laloë, J. Phys. I France **5**, 1255 (1995).
39. F. Laloë, in *Bose-Einstein condensation*, edited by A. Griffin, D. Snoke, S. Stringari (Cambridge University Press, 1993).
40. A.A. Abrikosov, L.P. Gorkov, I.E. Dialoshinski, *Methods of quantum field theory in statistical physics* (Dover Publications, 1963).
41. R.P. Feynman, *Statistical mechanis, a set of lectures* (Frontiers in Physics, Benjamin, 1972).
42. Veit Elser, Ph.D. Thesis, *Topics in Statistical Mechanics*, 1984.
43. W. Krauth, Phys. Rev. Lett. **77**, 3695 (1997).
44. J.E. Robinson, Phys. Rev. **83**, 678 (1951).
45. P. Grüter, F. Laloë, A.E. Meyerovich, W. Mullin, J. Phys. I France **7**, 485 (1997).
46. R. Spector (private communication).
47. A.Z. Patashinskii, V.L. Pokrovskii, J. Exptl. Theoret. Phys. (USSR) **46**, 994 (1964); Soviet Phys. JETP **19**, 677 (1964).
48. Ph. Courteille, R.S. Freeland, D.J. Heinzen, F.A. Abeelen, B.J. Verhaar, Phys. Rev. Lett. **81**, 69 (1998).
49. L. You, *Contribution to the BEC conference at the ITP* (University of California, Santa Barbara, 1998); M. Marinescu, L. You (preprint).
50. S. Inouye, M.R. Andrews, J. Stenger, H.-J. Miesner, D.M. Stamper-Kurn, W. Ketterle, Nat. **392**, 151 (1998).
51. G. Baym, D. Vautherin, J.P. Blaizot, M. Holzmann, F. Laloë, Phys. Rev. Lett. (to be published).